NUMERICAL INVESTIGATION OF AEROELASTIC RESPONSE OF WINGS USING UNSTEADY VORTEX LATTICE METHOD

A THESIS SUBMITTED TO
THE GRADUATE SCHOOL OF NATURAL AND APPLIED SCIENCES
OF
MIDDLE EAST TECHNICAL UNIVERSITY

BY

ALI OSMAN FIRAT

IN PARTIAL FULFILLMENT OF THE REQUIREMENTS
FOR
THE DEGREE OF MASTER OF SCIENCE
IN
AEROSPACE ENGINEERING

APRIL 2025

Approval of the thesis:

NUMERICAL INVESTIGATION OF AEROELASTIC RESPONSE OF WINGS USING UNSTEADY VORTEX LATTICE METHOD

submitted by **ALI OSMAN FIRAT** in partial fulfillment of the requirements for the degree of **Master of Science in Aerospace Engineering Department, Middle East Technical University** by,

Prof. Dr. Naci Emre ALTUN
Dean, Graduate School of **Natural and Applied Sciences** _____

Prof. Dr. Serkan ÖZGEN
Head of Department, **Aerospace Engineering** _____

Assoc. Prof. Dr. Nilay SEZER UZOL
Supervisor, **Aerospace Engineering, METU** _____

Examining Committee Members:

Assoc. Prof. Dr. Mustafa PERÇİN
Aerospace Engineering, METU _____

Assoc. Prof. Dr. Nilay SEZER UZOL
Aerospace Engineering, METU _____

Assoc. Prof. Dr. Melin ŞAHİN
Aerospace Engineering, METU _____

Assoc. Prof. Dr. Elif OĞUZ
Civil Engineering, METU _____

Assist. Prof. Dr. Onur BAŞ
Mechanical Engineering, TED University _____

Date:10.04.2025

I hereby declare that all information in this document has been obtained and presented in accordance with academic rules and ethical conduct. I also declare that, as required by these rules and conduct, I have fully cited and referenced all material and results that are not original to this work.

Name, Surname: Ali Osman FIRAT

Signature :

ABSTRACT

NUMERICAL INVESTIGATION OF AEROELASTIC RESPONSE OF WINGS USING UNSTEADY VORTEX LATTICE METHOD

FIRAT, Ali Osman
M.S., Department of Aerospace Engineering
Supervisor: Assoc. Prof. Dr. Nilay SEZER UZOL

April 2025, 92 pages

This thesis presents an in-depth investigation of nonlinear aeroelastic phenomena, specifically focusing on flutter behavior in flexible wing-like structures. A novel computational analysis tool is developed by integrating the Unsteady Vortex Lattice Method (UVLM) for predicting unsteady aerodynamic loads with the Finite Element Method (FEM) for analyzing structural dynamics. The study utilizes comprehensive time-domain simulations to capture the fully nonlinear fluid-structure interactions essential for accurately predicting flutter onset and subsequent aeroelastic response.

Initially, the thesis provides an overview of foundational aeroelastic theory and classical frequency-domain methods, emphasizing their shortcomings in capturing complex nonlinear behaviors. Subsequently, the coupling approach between UVLM and FEM is detailed, including mathematical formulations, discretization methods, and iterative solution strategies to ensure accuracy and stability. To validate the developed computational model, well-documented benchmark cases, such as experiments involving two-degree-of-freedom (2-DOF) flat plates in low-speed wind tunnel setups, are analyzed. The numerical results exhibit strong alignment with experimental observations, particularly in predicting critical flutter conditions and aeroelastic re-

sponses.

Finally, the thesis explores potential applications of the validated analysis method to more complex structural configurations, demonstrating its utility for examining design parameters, stability limits, and flutter mitigation techniques relevant to modern aerospace structures. The outcomes significantly enhance the understanding of nonlinear aeroelastic behavior, providing a robust and efficient computational framework for future aeroelastic analysis and aerospace engineering design applications.

Keywords: Aeroelasticity, Vortex Lattice Method, Flutter Analysis, Thin Airfoil

ÖZ

KANATLARIN AEROELASTİK TEPKİLERİNİN ZAMANA BAĞLI GİRDAP KAFES YÖNTEMİ İLE SAYISAL OLARAK İNCELENMESİ

FIRAT, Ali Osman
Yüksek Lisans, Havacılık ve Uzay Mühendisliği Bölümü
Tez Yöneticisi: Doç. Dr. Nilay SEZER UZOL

Nisan 2025 , 92 sayfa

Bu tez çalışması, esnek kanat benzeri yapılarda görülen doğrusal olmayan aeroelastik davranışları, özellikle çırpınma olayını ayrıntılı olarak ele almaktadır. Çalışmada, aerodinamik yükleri hesaplamak için zamana bağlı Girdap Kafes Metodu (GKM) ve yapısal dinamikleri incelemek için Sonlu Elemanlar Metodu (SEM) birleştirilerek özgün bir hesaplamalı analiz aracı geliştirilmiştir. Tam doğrusal olmayan akışkan-yapı etkileşimlerini yakalamak ve çırpınma başlangıcını hassas bir biçimde tahmin etmek amacıyla zamana dayalı simülasyonlar gerçekleştirilmiştir.

Tezin ilk bölümlerinde, klasik aeroelastik teoriler ve geleneksel frekans tabanlı analiz yöntemleri gözden geçirilmiş, bu yöntemlerin doğrusal olmayan karmaşık davranışları tam anlamıyla açıklamadaki yetersizlikleri vurgulanmıştır. Daha sonra, geliştirilen GKM-SEM çift yönlü etkileşim stratejisi ayrıntılı olarak anlatılmış; matematiksel formülasyonlar, ayrıklaştırma teknikleri ve çözümün doğruluğunu ve kararlılığını sağlayan iteratif yaklaşımlar ele alınmıştır. Sayısal modelin doğruluğunu test etmek için, literatürde iyi bilinen düşük hızlı rüzgâr tüneli deneyleri kullanılarak iki serbestlik dereceli (2-SD) düz levha üzerindeki test durumları incelenmiş, hesaplanan

çırpınma koşulları ile deneysel veriler arasındaki uyum ortaya konmuştur.

Son olarak, doğrulanmış bu analiz yönteminin daha karmaşık yapı ve akış koşullarına nasıl uyarlanabileceği tartışılmış, gelecekteki hava araçları için aeroelastik kararsızlıkların incelenmesi ve önlenmesinde güvenilir bir araç sağlandığı gösterilmiştir. Bu tez, doğrusal olmayan aeroelastik davranışın anlaşılmasına önemli katkılar sağlamakta ve havacılık mühendisliği tasarım süreçleri için hızlı ve güvenilir bir hesaplama aracı sunmaktadır.

Anahtar Kelimeler: Aeroelastisite, Girdap Kafes Yöntemi, Çırpınma Analizi, İnce Kanat Kesiti

To my wife, whose steadfast support enabled me to pursue this endeavor; to my mother and dad whose confidence in my abilities continually motivated my progress, I dedicate this work.

ACKNOWLEDGMENTS

I am immensely grateful to my supervisor, Assoc. Prof. Dr. Nilay SEZER UZOL, for her invaluable guidance, insightful feedback, and unwavering support throughout this journey.

TABLE OF CONTENTS

ABSTRACT v

ÖZ vii

ACKNOWLEDGMENTS x

TABLE OF CONTENTS xi

LIST OF TABLES xv

LIST OF FIGURES xvi

LIST OF ABBREVIATIONS and SYMBOLS xix

CHAPTERS

1 INTRODUCTION 1

1.1 Introduction to Aeroelasticity 1

1.2 Historical Development and Early Aeroelastic Failures 5

1.3 Theoretical Foundations and Collar's Aeroelastic Triangle 8

1.4 Frequency-Domain Analysis and Classical Linear Aeroelastic Theories 11

1.5 Limitations of Linear Aeroelastic Theories 13

1.6 Nonlinear Aeroelasticity: Concepts and Practical Examples 16

1.7 Limit Cycle Oscillations (LCOs): Mechanisms and Implications . . . 19

1.8 Computational Aeroelasticity and Fluid-Structure Interaction (FSI) . 21

1.9 Current State-of-the-Art and Research Gaps 24

1.10 Motivation and Objectives of the Thesis 27

1.11 Outline of the Thesis 29

2 METHODOLOGY 31

2.1 Methodology for Aerodynamic Analysis 33

2.1.1 Unsteady Vortex Lattice Method (UVLM) 33

2.1.2 UVLM Panel Discretization 34

2.1.3 Governing Equations and Boundary Conditions 35

2.1.4 Numerical Solution Methodology: Solving for Γ 36

2.1.5 Aerodynamic Forces and Moments 37

2.1.6 Comparison of Vortex Core Models 38

2.2 Methodology for Structural Analysis 40

2.2.1 Meshing 41

2.2.2 Finite Element Matrices 42

2.3 Methodology for Coupled Aerodynamic/Structural Analysis 42

2.3.1 Understanding Plunge and Pitch Motion in Aeroelasticity . . . 43

2.3.2 Equations of Motion for Plunge and Pitch 44

2.3.3 Aerodynamic and Structural Coupling 44

2.3.4 Finite Element Method for Structural Dynamics 45

2.4 Discretization of Structural Domain and Mesh Size Study 46

2.4.1 Boundary Conditions 47

2.5 Coupling with Aerodynamics Analysis 49

Matrix Form Representation: 50

State-Space Formulation: 50

2.5.1 Coupling Mechanism Between Structure and Aerodynamics . 51
2.6 Numerical Implementation 51
Wake Dynamics and UVLM Integration: 52
2.7 Stability and Flutter Analysis 53
Validation Cases: 53
2.8 Summary 54
3 VALIDATION SIMULATIONS AND RESULTS 55
3.1 2-D/3-D Validation Studies for Aerodynamic Analysis 56
3.1.1 2-D Airfoil (Flat Plate): Steady-State Test Case 56
3.1.2 2-D Airfoil (Flat Plate): Unsteady Test Case 57
Circulatory vs. Non-Circulatory Lift Contributions: 58
Theodorsen's Function: 58
3.1.2.1 Results and Discussions 59
3.1.3 3-D Wing: Steady-State Test Case 65
3.1.3.1 Lift Calculations 65
3.2 Validation Studies for Structural Analysis: Steady-State Test Case . . 67
3.2.1 Analytical Beam Theory Approach 67
3.2.2 Finite-Element Analyses: ABAQUS CAE Model 68
3.2.3 Finite-Element Analyses: In-house FEM Code Model 68
3.2.4 Results and Discussions 69
3.3 Validation Studies for Aeroelastic Analysis: Unsteady Test Case . . . 70
Computational Simulations and Parameters: 71
Numerical Methodology: 72

3.3.1 Results for Flutter Analysis 72

3.4 Summary and Discussions 74

4 AEROELASTIC APPLICATIONS AND RESULTS 77

4.1 Flutter Analysis of a Clamped-Wing Configuration 78

4.2 External Mass Attachment Study 80

4.3 Chapter Summary and Concluding Remarks 84

5 CONCLUSION AND FUTURE WORK 87

5.1 Future Work Suggestions 88

REFERENCES 89

LIST OF TABLES

TABLES

Table 3.1 Simulation parameters 71

Table 4.1 Plate material and geometric parameters 79

Table 4.2 Physical properties of the plate and store 81

Table 4.3 Natural frequencies of the first three modes for different store locations 81

Table 4.4 Predicted flutter speeds and frequencies for different store locations . 83

LIST OF FIGURES

FIGURES

Figure 1.1 Collar's Triangle of Aeroelasticity, showing the interaction between aerodynamic forces, elasticity, and inertia. Each side of the triangle represents different aeroelastic phenomena, with arrows indicating interactions [1]. 4

Figure 2.1 Representation of an aeroelastic wing model showing surface panels, wake panels, and collocation points for aerodynamic force calculations, adapted from [2]. 35

Figure 2.2 Kutta condition usage, adapted from [2]. 35

Figure 2.3 Lift components due to plunging and pitching motions [3]. . . . 38

Figure 2.4 Comparison of Vortex Core Models 40

Figure 2.5 Finite element mesh of a thin rectangular plate 41

Figure 2.6 Lift components due to bending and torsion motions [3]. 43

Figure 2.7 Model for plunge and pitch motion [4]. 44

Figure 2.8 Finite element representation of a thin rectangular plate, illustrating clamped and free edges. 48

Figure 2.9 Aeroelastic model with 2-DoF system, adapted from [5]. 49

Figure 2.10 Two-way coupling mechanism between structural and aerodynamic solvers. 51

Figure 3.1 Comparison of lift coefficients for a pitching airfoil (k = 0.25): Theodorsen's (analytical), Circulatory UVLM ($C_{L,\text{circ}}$), Non-Circulatory UVLM ($C_{L,\text{nc}}$), Total UVLM. 60

Figure 3.2 Comparison of lift coefficients for a pitching airfoil (k = 0.5): Theodorsen's (analytical), Circulatory UVLM ($C_{L,\text{circ}}$), Non-Circulatory UVLM ($C_{L,\text{nc}}$), Total UVLM. 60

Figure 3.3 Comparison of lift coefficients for a pitching airfoil (k = 0.75): Theodorsen's (analytical), Circulatory UVLM ($C_{L,\text{circ}}$), Non-Circulatory UVLM ($C_{L,\text{nc}}$), Total UVLM. 61

Figure 3.4 Lift coefficient for pitching airfoil for k=0.25 61

Figure 3.5 Lift coefficient for pitching airfoil for k=0.5 62

Figure 3.6 Lift coefficient for pitching airfoil for k=0.75 62

Figure 3.7 Wake formation for reduced frequency is zero (no oscillation) and time step is 0.002. 63

Figure 3.8 Wake formation for reduced frequency is 0.1 and time step is 0.002 with small amplitude. 64

Figure 3.9 Wake formation for reduced frequency is 0.4 and time step is 0.002 with small amplitude. 64

Figure 3.10 Wake formation for reduced frequency is 0.8 and time step is 0.002 with small amplitude. 65

Figure 3.11 ABAQUS CAE deflection contour showing a maximum tip displacement of about $45\,\text{mm}$. 69

Figure 3.12 Independent FEM code deflection result, with a maximum tip displacement near $44.66\,\text{mm}$. 70

Figure 3.13 Time history of plunging motion 73

Figure 3.14 Time history of pitching motion 73

Figure 3.15 Free wake demonstration after the flutter speed. 74

Figure 3.16 Free wake demonstration after the flutter speed. 74

Figure 4.1 First three mode shapes of the clamped-wing configuration. . . . 79

Figure 4.2 Time history of tip displacement 79

Figure 4.3 Time history of twist angle 80

Figure 4.4 Plate geometry, boundary conditions, and store attachment locations X_s. 82

Figure 4.5 Mode shapes for clean configuration 82

Figure 4.6 Time history of twist angle without extra mass 83

Figure 4.7 Time history of tip displacement without extra mass 84

Figure 4.8 Time history of tip displacement with extra masses at different store locations 84

LIST OF ABBREVIATIONS and SYMBOLS

ABBREVIATIONS

AoA	Angle of Attack
CFD	Computational Fluid Dynamics
CG	Center of Gravity
DLM	Doublet-Lattice Method
DMD	Dynamic Mode Decomposition
EA	Elastic Axis
FEM	Finite Element Method
FSI	Fluid-Structure Interaction
LCO	Limit Cycle Oscillation
POD	Proper Orthogonal Decomposition
ROM	Reduced-Order Model
UAS	Unmanned Aerial Systems
UAV	Unmanned Air Vehicle
UVLM	Unsteady Vortex Lattice Method

SYMBOLS

a	Vortex Core Radius
A	Cross-Sectional Area of Beam
A	Amplitude
$\mathbf{A}$	Influence Coefficient Matrix
AR	Aspect Ratio of Wing
b	Span

$\mathbf{b}$	Known RHS Vector
c	Chord Length
c	Damping
$\mathbf{C}$	Damping Matrix
C_d	Drag Coefficient
C_k	Theodorsen's Function
C_l	Lift Coefficient
dl	Vortex Segment Length
E	Young's Modulus
EI	Flexural Rigidity of Beam
$\mathbf{F}$	Aerodynamic Force
h	Plunge Displacement
h	Plate Thickness
I	Second Moment of Inertia
$\mathbf{I}$	Identity Matrix
k	Reduced Frequency
k	Stiffness
$\mathbf{K}$	Stiffness Matrix
L	Lift
m	Mass per Unit Span
M	Total Mass
$\mathbf{M}$	Mass Matrix
$\mathbf{M}$	Aerodynamic Pitching Moment
$\mathbf{M}$	Mach Number
$\mathbf{n}$	Normal Vector
$\mathbf{Q}(k)$	Aerodynamic Influence Coefficient Matrix
q	Dynamic Pressure

$\mathbf{r}$	Distance Vector
Re	Reynolds Number
S	Planform Area of Wing
S_α	Static Moment of Flat-Plate Model about Elastic Axis
t	Airfoil Thickness
$\mathbf{u}(x,t)$	Displacement Vector
U	Freestream Velocity
$\mathbf{U}$	Velocity Vector
$\mathbf{v}$	Velocity Vector
$\mathbf{V}$	Velocity Vector
w	Uniform Load
X_{CG}	Position of Center of Gravity
α	Angle of Attack
α	Pitch Amplitude
δ	Deflection
ϕ	Velocity Potential
Γ	Circulation
ω	Frequency
ρ	Density
ζ	Damping Ratio

CHAPTER 1

INTRODUCTION

1.1 Introduction to Aeroelasticity

Aeroelasticity is the study of the complex and critical interactions between aerodynamic forces Fig. 1.1, structural flexibility, and inertial dynamics. These interactions, which occur continuously and simultaneously during flight, significantly affect the performance, safety, and structural integrity of all aerospace vehicles, including commercial aircraft, military jets, unmanned aerial vehicles (UAVs), and even spacecraft structures. Since the earliest days of aviation, aeroelasticity has played a crucial role in aircraft design and has been integral to ensuring operational safety. Its importance is underscored by numerous historical incidents, where the lack of adequate aeroelastic understanding resulted in catastrophic structural failures and significant losses of life and resources [6, 7]. To understand aeroelastic phenomena comprehensively, one must explicitly consider the three primary interacting domains: aerodynamic loading, structural elasticity, and inertial properties. Aerodynamic forces arise due to the interaction between an aircraft structure and the surrounding airflow. These forces continuously fluctuate depending on flight speed, angle of attack, and structural geometry changes during maneuvers or external disturbances such as gusts. Structural elasticity describes the deformable nature of aircraft structures, which are designed intentionally lightweight to maximize flight performance and fuel efficiency. Consequently, this inherent flexibility introduces complexity, as structural deformation directly affects aerodynamic forces. Finally, inertial forces related to the mass distribution and dynamic response of the structure also significantly influence aeroelastic behavior, particularly during rapid maneuvers or transient loading events such as gust encounters [8, 3]. Historically, the critical importance of aeroelastic phenomena

became apparent early in aviation history through various structural failures. One notable example, widely cited in both aeroelastic and structural engineering literature, is the collapse of the Tacoma Narrows Bridge in 1940. Though not an aircraft, this landmark event is frequently discussed within aeroelastic contexts because it clearly demonstrated the catastrophic consequences of self-excited aerodynamic instabilities on flexible structures. Aeroelastic principles uncovered from analyzing this failure subsequently informed aviation structural design practices, emphasizing the necessity of explicitly considering aerodynamic interactions in structural engineering across various domains [9]. In aviation itself, the destructive potential of aeroelastic phenomena was tragically demonstrated by several catastrophic incidents throughout the early mid-20th century. Perhaps the most wellknown aeroelastic instability is flutter a violent, self-excited vibration caused by aerodynamic forces interacting dynamically with structural modes of vibration. Flutter can rapidly escalate structural oscillations to amplitudes far exceeding structural limits, leading to dramatic structural failures. Such failures in early aircraft were often sudden and unexpected, as the aeroelastic principles governing flutter were not yet fully understood. These catastrophic events compelled engineers to rigorously investigate aeroelastic phenomena, initiating a systematic effort toward understanding, modeling, and predicting aeroelastic behaviors explicitly and accurately [1, 10]. The significance of aeroelasticity has not diminished over time. Instead, it has intensified as modern aircraft designs pursue ever-increasing performance capabilities, including higher speed, greater efficiency, and lighter structural configurations. Modern design practices frequently incorporate high aspect ratio wings, lightweight composite materials, and novel configurations explicitly tailored for enhanced fuel economy and operational flexibility. However, these desirable aerodynamic and structural characteristics explicitly increase vulnerability to aeroelastic instabilities such as flutter, divergence, and control reversal, thus presenting ongoing challenges to aircraft designers and aerospace engineers. Consequently, modern aerospace engineering explicitly requires increasingly sophisticated analysis tools capable of accurately capturing and predicting these complex aeroelastic behaviors, ensuring structural integrity and operational safety across all flight regimes [11, 12]. Aeroelastic phenomena are not confined solely to flutter, although flutter remains one of the most critical and widely studied aeroelastic instabilities. Divergence, another critical phenomenon, occurs when

steady aerodynamic loading explicitly exceeds structural stiffness, causing structural deformation to escalate continuously, potentially leading to catastrophic structural failure. Another significant aeroelastic phenomenon, control reversal, explicitly describes situations where aerodynamic loading on flexible structures causes control surfaces, such as ailerons or elevators, to deflect in opposite directions from intended commands, significantly impairing aircraft control and stability. Collectively, these phenomena explicitly emphasize the breadth and depth of aeroelastic challenges and the necessity for comprehensive and accurate predictive modeling methods in aircraft design [8, 3, 13]. Explicitly recognizing these aeroelastic challenges, the field of aeroelasticity has evolved significantly through theoretical, experimental, and computational advancements. Early theoretical foundations laid down by pioneers such as Collar, Theodorsen, and Bisplinghoff provided essential analytical frameworks, explicitly enabling engineers to predict and mitigate aeroelastic instabilities. With the advent of computational technology, modern computational aeroelasticity explicitly integrates advanced aerodynamic and structural models, explicitly coupled through numerical fluid-structure interaction techniques. This approach enables detailed and realistic simulation of complex aeroelastic phenomena, explicitly capturing nonlinear behaviors, transient dynamics, and large structural deformations explicitly observed in contemporary aerospace structures [6, 7, 14]. Today, aeroelastic analysis explicitly constitutes a critical stage in aircraft design and certification processes. Regulatory bodies, including the Federal Aviation Administration (FAA) and the European Union Aviation Safety Agency (EASA), explicitly require rigorous aeroelastic analyses as part of aircraft certification, explicitly underscoring aeroelasticity's critical role in ensuring flight safety and structural reliability. Therefore, ongoing advancements explicitly aimed at improving aeroelastic modeling accuracy, predictive capabilities, and computational efficiency remain essential tasks explicitly at the forefront of aerospace research and development [15, 16]. This thesis explicitly contributes to addressing these ongoing aeroelastic challenges by developing, validating, and applying a robust, computational aeroelastic analysis framework explicitly designed to capture complex nonlinear aeroelastic behaviors accurately. The comprehensive computational methodology developed explicitly integrates aerodynamic modeling using the Unsteady Vortex Lattice Method (UVLM), structural modeling using the Finite Element Method (FEM), and explicit coupling of these two domains within a robust

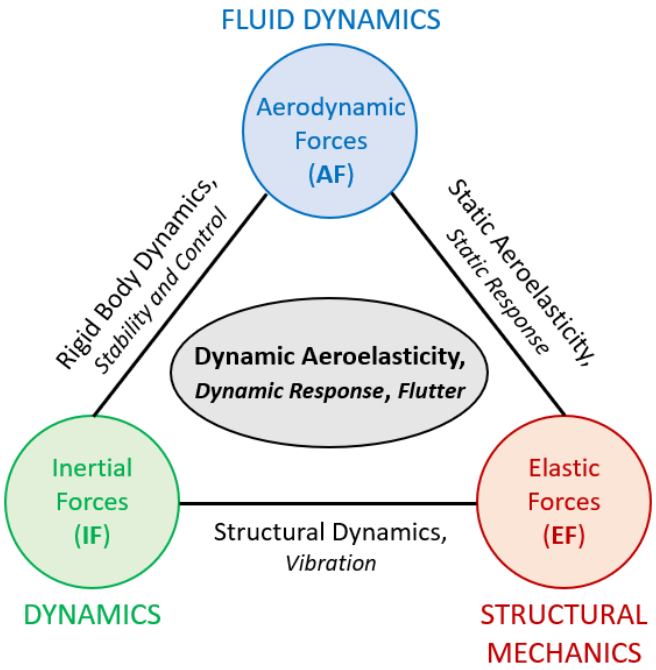

Figure 1.1: Collar's Triangle of Aeroelasticity, showing the interaction between aerodynamic forces, elasticity, and inertia. Each side of the triangle represents different aeroelastic phenomena, with arrows indicating interactions [1].

time-domain fluid-structure interaction solver. The outcomes of this research explicitly aim to enhance aeroelastic prediction capabilities, providing aerospace engineers with explicitly powerful analytical tools to ensure aircraft structural integrity, operational safety, and superior flight performance. In summary, aeroelasticity remains a critical and continually evolving area within aerospace engineering explicitly addressing the dynamic interactions between aerodynamic forces, structural flexibility, and inertial effects. Understanding, accurately modeling, and effectively mitigating aeroelastic phenomena explicitly remain essential to ensuring safety, reliability, and performance in modern aviation. This thesis explicitly and systematically addresses critical aeroelastic challenges through advanced computational modeling explicitly aligned with contemporary aerospace engineering demands and practices.

1.2 Historical Development and Early Aeroelastic Failures

The historical development of aeroelasticity has been fundamentally shaped by a sequence of pivotal events, theoretical breakthroughs, and catastrophic structural failures. From the earliest years of aviation, engineers encountered unexpected aerodynamic-structural interactions that significantly influenced aircraft performance, often resulting in disastrous outcomes. These early encounters with aeroelastic phenomena compelled researchers to initiate systematic studies to understand, quantify, and ultimately mitigate their adverse effects. The lessons drawn from these historical aeroelastic failures explicitly provided the foundation upon which modern aeroelastic theories and practices are built [6, 1, 17]. Early aviation was characterized by extensive trial and error, with engineers pushing structural designs to higher speeds and lighter weights without fully grasping the potential implications of aeroelastic interactions. Among the earliest documented cases illustrating aeroelastic instability was the phenomenon known as flutter, wherein structural vibration modes resonated destructively with aerodynamic forces, causing rapid and violent structural oscillations. Early observations of flutter date back to World War I, where several military aircraft exhibited unexplained structural failures in flight, particularly affecting wing structures and tail assemblies. Engineers, at first baffled by these sudden and violent failures, soon recognized a correlation between increased flight speeds, structural flexibility, and

structural failure, though initially lacking the analytical tools necessary for rigorous prediction and mitigation [10, 18]. A landmark event often cited in aeroelastic literature was the catastrophic structural failure of the British Handley Page O/400 bomber during World War I. This incident dramatically illustrated the destructive potential of flutter, as structural oscillations rapidly escalated beyond design limits. Investigations into this failure were among the earliest systematic studies explicitly linking structural vibrations and aerodynamic forces. As aircraft speeds increased during the 1920s and 1930s, similar incidents of flutter-induced structural failures continued to emerge, prompting more detailed theoretical and experimental research explicitly dedicated to understanding and predicting aeroelastic phenomena [6, 3]. A significant theoretical milestone explicitly addressing early aeroelastic problems was achieved in 1924 by Frederick Bramwell. Bramwell explicitly described flutter as a resonance phenomenon, clearly identifying that structural oscillations could be amplified by aerodynamic forces if structural natural frequencies coincided with aerodynamic excitation frequencies. His work explicitly marked the first clear theoretical recognition of flutter, laying the groundwork for more rigorous analytical approaches. However, Bramwell's early theoretical framework was primarily qualitative and lacked the explicit mathematical rigor needed to predict flutter accurately. Nevertheless, his foundational contributions significantly influenced subsequent aeroelastic research explicitly throughout the early-to-mid 20th century [10, 1]. Further advancing aeroelastic understanding, Sir Sydney Goldstein in the 1930s explicitly initiated systematic analytical and experimental investigations into aeroelastic instability. Goldstein's pioneering work provided valuable insights into the physical mechanisms underlying aeroelastic phenomena and demonstrated the necessity of explicitly accounting for aerodynamic-structural coupling in aircraft design. Goldstein's early efforts, although limited by the analytical and experimental tools of his era, clearly indicated the complexity of aeroelastic interactions and explicitly paved the way for more sophisticated theoretical developments that would follow [18, 6]. The most transformative theoretical advancement in aeroelasticity during this period was undoubtedly Theodore Theodorsen's groundbreaking research published in 1935. Theodorsen explicitly introduced an analytical approach to predicting flutter and other aeroelastic phenomena by mathematically describing the aerodynamic forces acting on oscillating airfoils. His now-famous Theodorsen function explicitly relates unsteady aerodynamic lift

forces to structural oscillation frequencies, enabling quantitative and predictive flutter analyses explicitly for the first time. Theodorsen's formulation, explicitly rooted in linear unsteady aerodynamic theory, significantly enhanced engineers' abilities to understand, analyze, and mitigate aeroelastic instabilities explicitly in aviation [19, 3]. Despite these theoretical advancements, catastrophic aeroelastic failures continued to occur during the mid-20th century, as aviation increasingly pursued higher operational speeds, lighter structures, and more flexible airframe designs. One of the most notorious incidents explicitly demonstrating catastrophic aeroelastic instability in civil engineering—though widely discussed within aeroelastic literature—was the collapse of the Tacoma Narrows Bridge in 1940. While not an aircraft failure per se, this dramatic event vividly illustrated aeroelastic instability principles in flexible structures exposed to aerodynamic loading. Engineers explicitly recognized the collapse as a clear demonstration of self-excited oscillations akin to flutter, emphasizing the broader relevance of aeroelastic principles beyond purely aeronautical contexts. This incident further motivated aeroelastic research explicitly across disciplines, emphasizing the universal importance of explicitly addressing aeroelastic phenomena in flexible structural designs [9, 6]. In aviation itself, multiple military and civilian aircraft incidents explicitly highlighted the continued importance of accurate aeroelastic prediction. A notable military example explicitly includes the structural failures of early jet aircraft prototypes during high-speed tests in the post-World War II era. These failures explicitly demonstrated limitations of existing linear frequency-domain flutter theories, especially at transonic and supersonic speeds, where aerodynamic nonlinearities, shock waves, and large structural deformations explicitly occur. These incidents explicitly underscored the urgency of developing more advanced theoretical and computational tools explicitly capable of capturing nonlinear aeroelastic behaviors more accurately [7, 8, 11]. Responding to these challenges, the mid-to-late 20th century explicitly witnessed remarkable theoretical, experimental, and computational advancements in aeroelastic research explicitly driven by real-world needs. Pioneering efforts by Collar, Bisplinghoff, Ashley, and others explicitly resulted in comprehensive theoretical frameworks explicitly capable of predicting various aeroelastic phenomena, explicitly including flutter, divergence, and control reversal. Concurrently, experimental techniques explicitly evolved, enabling systematic aeroelastic testing explicitly under controlled laboratory conditions, significantly enhancing un-

derstanding of aeroelastic phenomena [1, 6, 17]. Ultimately, the historical trajectory explicitly described in this section illustrates the critical importance of aeroelasticity explicitly shaped by real-world aeroelastic failures and theoretical advances explicitly developed in response to these incidents. Early catastrophic events explicitly underscored the need for rigorous aeroelastic research explicitly aimed at preventing structural failures and improving flight safety. These historical lessons continue to inform modern aerospace engineering explicitly, guiding ongoing advancements explicitly aimed at accurately predicting, mitigating, and managing aeroelastic phenomena explicitly across the spectrum of aerospace applications.

1.3 Theoretical Foundations and Collar's Aeroelastic Triangle

The systematic theoretical understanding of aeroelastic phenomena was significantly advanced by Arthur Collar's seminal contributions in the mid-20th century, notably through his conceptual framework known as Collar's Aeroelastic Triangle. This concept, explicitly introduced by Collar in 1946, provided aerospace engineers a clear and intuitive representation of the complex interactions between aerodynamic forces, structural elasticity, and inertial dynamics. Collar's triangle explicitly describes these three interacting domains as sides of a triangle, visually representing how they interact to produce various aeroelastic phenomena, most notably flutter, divergence, and control reversal [1, 6, 8]. Explicitly, Collar's Aeroelastic Triangle comprises three distinct but interconnected domains: aerodynamics, elasticity, and inertia. Each domain represents a critical aspect explicitly influencing aeroelastic behavior. Aerodynamic forces explicitly arise from fluid–structure interactions during flight, influenced by the aircraft's shape, speed, angle of attack, and structural deformation. Structural elasticity explicitly accounts for the flexibility and deformability of the structure, determined by material properties, geometric configuration, and structural stiffness distribution. Finally, inertia explicitly relates to the mass distribution and dynamic response characteristics of the structure, particularly significant in transient dynamic scenarios such as gust encounters or rapid maneuvers [1, 3]. The explicit interactions between these three domains manifest various critical aeroelastic phenomena. One well-known phenomenon explicitly explained by Collar's triangle is flutter, charac-

terized by self-sustained oscillations occurring due to a dynamic coupling between aerodynamic forces and structural modes of vibration. Divergence, another significant aeroelastic instability, explicitly occurs when aerodynamic loads exceed structural stiffness, leading to uncontrollable static deformation of the structure. Control reversal explicitly describes scenarios in which aerodynamic loads alter the structural deflections in such a manner that control surfaces become ineffective or behave contrary to the intended control inputs. Each of these phenomena explicitly involves unique interactions among the aerodynamic, elastic, and inertial forces represented clearly by Collar's Aeroelastic Triangle [6, 8, 3]. Flutter explicitly provides one of the clearest examples illustrating the intricate interplay of these three domains. Explicitly, aerodynamic forces acting on a flexible structure can dynamically couple with structural vibration modes at specific flight speeds or operating conditions. Explicitly, if aerodynamic forces impart sufficient energy into these structural vibrations, oscillations can rapidly amplify, potentially leading to catastrophic structural failures. Crucially, the explicit inertial characteristics of the structure significantly influence flutter characteristics, as structural mass distribution directly affects the natural frequencies and mode shapes involved in these dynamic interactions. Structural elasticity explicitly determines how deformation occurs, further influencing aerodynamic loads in a continuously interacting loop explicitly captured by Collar's Triangle representation [19, 1, 7]. Collar's Triangle explicitly played a pivotal role in shaping theoretical approaches to aeroelastic analyses by providing a clear conceptual basis explicitly connecting the physical mechanisms involved in aeroelastic phenomena. This explicit clarity enabled engineers to develop systematic analytical methods for predicting and mitigating aeroelastic instabilities. Notably, Collar's theoretical work explicitly complemented earlier contributions by Theodore Theodorsen, whose groundbreaking aerodynamic theory explicitly quantified unsteady aerodynamic forces acting on oscillating airfoils. The explicit combination of Collar's conceptual framework with Theodorsen's rigorous aerodynamic formulations provided engineers with powerful analytical tools explicitly facilitating reliable prediction and management of aeroelastic phenomena explicitly encountered in aircraft design [19, 1, 6]. Throughout the mid-to-late 20th century, Collar's Aeroelastic Triangle explicitly served as the foundational conceptual model for numerous theoretical advancements in aeroelasticity. Explicitly, scholars such as Bisplinghoff, Ashley, and Garrick extensively employed

Collar's conceptual framework to derive analytical solutions for classical aeroelastic problems explicitly, including flutter, divergence, and control reversal. Their collective efforts explicitly resulted in robust analytical methods explicitly capable of quantitatively predicting critical flutter speeds, structural deformation patterns, and stability boundaries explicitly across a range of aircraft configurations and flight conditions. These theoretical methods explicitly became essential tools explicitly in aircraft design processes, significantly enhancing structural reliability and operational safety [6, 17, 3]. Beyond explicit analytical predictions, Collar's theoretical framework explicitly influenced the experimental practices explicitly adopted in aeroelastic research. Experimental techniques explicitly evolved to systematically investigate interactions between aerodynamic forces, structural flexibility, and inertial properties, explicitly guided by the conceptual clarity explicitly provided by Collar's Triangle. Wind tunnel experiments, ground vibration tests, and flight tests explicitly designed to measure aeroelastic responses directly benefited from explicit conceptual understandings explicitly established by Collar's Triangle. These explicit experimental advancements significantly complemented theoretical analyses, explicitly providing essential validation data explicitly for analytical methods and computational tools explicitly developed throughout the latter half of the 20th century [7, 20, 8]. In contemporary aeroelasticity, Collar's Aeroelastic Triangle explicitly retains its conceptual significance, serving as an intuitive foundation explicitly for understanding complex aeroelastic interactions explicitly encountered in modern aerospace structures. Although explicit computational methods now dominate practical aeroelastic analyses explicitly due to their superior accuracy and versatility, Collar's conceptual framework explicitly remains invaluable explicitly for intuitive understanding, educational purposes, and preliminary analytical assessments explicitly in aerospace engineering practice. Explicitly, it continues to guide engineers explicitly in identifying critical aeroelastic interactions explicitly requiring further detailed analyses explicitly using advanced computational methods explicitly developed explicitly to address contemporary aeroelastic challenges explicitly [14, 12, 13].

1.4 Frequency-Domain Analysis and Classical Linear Aeroelastic Theories

Historically, aeroelastic phenomena have predominantly been analyzed using linear frequency-domain methods. These methods, developed extensively throughout the early-to-mid 20th century, rely on the assumption of linear structural behavior and small-amplitude harmonic oscillations. Such assumptions simplify the mathematical formulations significantly, allowing engineers to conduct swift analyses and preliminary evaluations of aeroelastic stability. Among these classical linear theories, Theodorsen's unsteady aerodynamic theory, along with the subsequently developed *p-k* and *g*-methods, remain particularly influential in aeroelastic literature due to their fundamental and practical importance [19, 6]. The cornerstone of linear frequency-domain aeroelastic analyses was provided by Theodore Theodorsen in 1935. Theodorsen developed an analytical framework to determine unsteady aerodynamic forces acting on harmonically oscillating airfoils under subsonic conditions. Central to his theory is the now-famous Theodorsen function, which relates the aerodynamic forces acting on an oscillating airfoil to the amplitude and frequency of its structural oscillations. This function accurately accounts for the effect of unsteady vortex shedding from the trailing edge, capturing the essential physical mechanisms underpinning aeroelastic instabilities, particularly flutter [19, 17]. Mathematically, Theodorsen's unsteady lift formulation is expressed as follows:

$$L(\omega) = \rho U^2 c \left[2\pi \left(i\frac{\omega h}{U} + \frac{c\dot{\alpha}}{2U} + \alpha \right) C(k) \right], \tag{1.1}$$

where $L(\omega)$ denotes the unsteady lift amplitude, ρ is the air density, U represents the freestream velocity, c is the airfoil chord length, h is the plunge displacement amplitude, and α denotes the pitch amplitude. The term $k = \frac{\omega c}{2U}$ represents the reduced frequency, and $C(k)$ is Theodorsen's complex aerodynamic function, which encapsulates the unsteady aerodynamic effects associated with trailing-edge vortex shedding [19, 6, 3]. Following Theodorsen's foundational theory, frequency-domain methods evolved to offer systematic and efficient procedures to predict aeroelastic stability boundaries, particularly the critical flutter speed. Among these approaches, Hassig's *p-k method*, introduced in the 1970s, gained considerable popularity due to its computational efficiency and straightforward application. The *p-k* method employs complex eigenvalue analyses to determine flutter instability points by examining the

aerodynamic damping and frequency characteristics as functions of the reduced frequency. Flutter occurs when aerodynamic damping transitions from positive (stabilizing) to negative (destabilizing), indicating that the aerodynamic forces amplify the structural oscillations rather than dampen them [21, 6]. Formally, the eigenvalue problem solved by the *p-k* method is represented as:

$$\left[-\omega^2\mathbf{M} + i\omega\mathbf{C} + \mathbf{K} - \frac{1}{2}\rho U^2\mathbf{Q}(k)\right]\mathbf{x} = 0, \tag{1.2}$$

where $\mathbf{M}$, $\mathbf{C}$, and $\mathbf{K}$ represent the mass, damping, and stiffness matrices of the structure, respectively, and $\mathbf{Q}(k)$ denotes the aerodynamic influence coefficient matrix computed at each reduced frequency k. The solution of this eigenvalue problem yields critical flutter speeds, mode shapes, and frequencies, providing essential information for preliminary aeroelastic design [6, 8]. Another significant advancement in frequency-domain analysis was Bendiksen's *g-method*, developed during the mid-1980s. The *g-method* generalizes the frequency-domain approach by allowing limited incorporation of nonlinear aerodynamic effects within an essentially linear structural framework. Bendiksen's formulation enhances prediction accuracy at moderately higher speeds where mild aerodynamic nonlinearities start influencing aeroelastic stability. Although fundamentally linear, this method marked an essential progression toward addressing nonlinear aeroelastic behaviors, particularly in transonic flight regimes [22, 3]. Despite their extensive historical usage and significant theoretical value, frequency-domain linear methods inherently exhibit limitations due to their underlying assumptions. Primarily, the linear theories assume structural deformations to remain small and aerodynamic forces proportional to these small displacements. Such assumptions prove increasingly restrictive as aircraft designs advance towards greater flexibility and higher operational speeds, where structural deformations may become large, and aerodynamic responses significantly nonlinear. At transonic and supersonic speeds, nonlinear phenomena such as shock waves, boundary-layer separation, and large structural deformations become prominent, thus rendering linear frequency-domain models inadequate [7, 23, 20]. Indeed, the transition to nonlinear phenomena becomes inevitable as aircraft design boundaries are extended. Nonlinear effects directly invalidate the linearizing assumptions inherent in frequency-domain methods, necessitating more sophisticated nonlinear analysis approaches. While linear methods remain invaluable in preliminary design phases and as pedagogical tools,

the reality of contemporary aircraft design dictates the use of time-domain and fully nonlinear computational techniques for accurate aeroelastic predictions [14, 11, 12]. In summary, classical frequency-domain aeroelastic theories, notably represented by Theodorsen's foundational theory and advanced by subsequent methods such as Hassig's *p-k* and Bendiksen's *g-method*, have profoundly influenced aeroelastic analysis and design practices. These methods have provided essential predictive tools for linear aeroelastic systems and formed the basis for modern aeroelastic analysis techniques. Nevertheless, the inherent limitations of these linear theories, particularly regarding their applicability to highly flexible and high-speed aircraft, underline the critical need for the development and application of nonlinear aeroelastic methodologies—topics explicitly addressed by the research presented in this thesis.

1.5 Limitations of Linear Aeroelastic Theories

Despite their historical significance and practical utility in early and mid-20th-century aeroelastic analyses, linear aeroelastic theories inherently possess critical limitations when applied to modern aircraft configurations. The assumptions underlying linear analyses—small-amplitude structural oscillations, linear aerodynamic force responses, and relatively rigid structural behavior—are increasingly invalidated by contemporary aerospace designs characterized by significant structural flexibility, nonlinear aerodynamic effects, and operations in high-speed flight regimes, including transonic and supersonic conditions [7, 23, 20]. The fundamental limitation of linear aeroelastic theories is the assumption of small structural displacements. Classical approaches, such as Theodorsen's aerodynamic theory and the frequency-domain eigenvalue methods, rely explicitly on linearized equations of motion. These formulations assume that structural deflections and the resulting aerodynamic responses remain infinitesimally small. While valid for low-speed, rigid or moderately flexible structures, these assumptions fail to capture realistic aeroelastic behaviors when structural deflections become substantial. Large structural deflections significantly alter aerodynamic loading distributions, producing nonlinearities that linear theories inherently cannot predict [8, 6]. At higher operational speeds, especially in the transonic and supersonic regimes, significant aerodynamic nonlinearities manifest, further challeng-

ing linear theory assumptions. The presence of shock waves, boundary-layer separation, vortex shedding, and complex flow interactions introduce strongly nonlinear aerodynamic forces. These nonlinear aerodynamic phenomena are not directly proportional to structural displacement or velocity, violating the fundamental assumptions of linear frequency-domain theories. Consequently, linear theories may significantly underestimate or inaccurately predict critical aeroelastic phenomena such as flutter onset speeds, structural response amplitudes, and stability boundaries under realistic operational conditions [13, 11]. A practical example demonstrating the inadequacy of linear theories at transonic speeds involves transonic flutter prediction. Linear aeroelastic methods typically predict flutter boundaries accurately in subsonic conditions, where aerodynamic nonlinearities are minimal. However, experimental and flight-test data explicitly reveal that at transonic speeds—typically Mach numbers between approximately 0.8 and 1.2—shock-induced aerodynamic nonlinearities considerably affect structural response and stability boundaries. For instance, nonlinear transonic effects often lead to flutter speeds differing substantially from those predicted by linear models. Such deviations can be critical for aircraft safety and certification, emphasizing the need for incorporating nonlinear aerodynamic effects explicitly within aeroelastic predictions [7, 24, 25]. Another significant limitation arises from the linear theories' inability to accurately predict nonlinear aeroelastic phenomena, notably limit cycle oscillations (LCOs). Unlike classical flutter, characterized by exponentially increasing oscillation amplitudes, LCOs stabilize at finite amplitudes due to nonlinear aerodynamic and structural interactions. Linear theories, inherently based on linear eigenvalue analyses, cannot capture amplitude-dependent damping effects and aerodynamic nonlinearities responsible for the stabilization of these oscillations. Consequently, linear methods often incorrectly predict either complete stability or unbounded instability, thereby misrepresenting the actual aeroelastic behavior of flexible aircraft wings undergoing moderate-to-large amplitude vibrations [23, 14, 11]. The emergence of lightweight composite materials and high-aspect-ratio wings in modern aircraft further exacerbates the limitations of linear theories. Composite structures often exhibit nonlinear material behavior and significant anisotropic stiffness characteristics. High-aspect-ratio wings, designed explicitly for fuel efficiency and performance optimization, inherently exhibit substantial flexibility, leading to significant nonlinear geometric effects due to large structural

deflections. Such nonlinear structural behaviors strongly affect aerodynamic load distributions, resulting in nonlinear aeroelastic responses poorly predicted by linear theories [12, 3]. Furthermore, linear aeroelastic analyses inadequately address transient phenomena that often arise from rapid maneuvers, gust encounters, or abrupt control surface inputs. These transient aeroelastic responses involve sudden large-amplitude deflections, nonlinear aerodynamic forces, and rapidly varying structural dynamics. Frequency-domain linear methods, by their nature, assume steady-state harmonic responses around equilibrium conditions and cannot directly capture such transient effects. Accurately predicting transient aeroelastic responses is essential, especially for agile military aircraft and unmanned aerial vehicles (UAVs), highlighting another critical shortcoming of traditional linear approaches [20, 26]. Recognizing these critical limitations, aeroelastic research progressively shifted toward nonlinear analytical and computational methodologies capable of capturing the complexities inherent in modern aerospace applications. Nonlinear computational methods, particularly those employing time-domain simulations, explicitly address large structural deformations, nonlinear aerodynamic effects, and transient aeroelastic interactions. Unlike frequency-domain linear methods, time-domain nonlinear approaches can simulate realistic aeroelastic responses under a wide variety of operational conditions, including transient maneuvers, gust encounters, and complex aerodynamic interactions [13, 26, 11]. To address the inherent deficiencies of linear aeroelastic theories, contemporary aeroelastic analysis often incorporates computational fluid dynamics (CFD), nonlinear structural analyses via the finite element method (FEM), and advanced fluid-structure interaction (FSI) coupling procedures. These methodologies explicitly capture large structural deflections, nonlinear aerodynamic loading distributions, transient aeroelastic phenomena, and limit cycle oscillations. As a result, these advanced computational techniques have become indispensable tools for accurately predicting aeroelastic stability, structural integrity, and operational safety in modern aircraft designs explicitly characterized by substantial flexibility and high operational speeds [13, 12, 14]. In conclusion, while linear frequency-domain aeroelastic theories historically provided critical analytical tools and fundamental understanding, their intrinsic limitations become increasingly apparent as aircraft designs evolve towards greater flexibility, higher speed regimes, and more pronounced aerodynamic nonlinearities. These limitations necessitate transitioning to nonlinear aeroelastic anal-

ysis methodologies capable of capturing realistic aeroelastic behaviors observed in modern aircraft configurations—a transition explicitly pursued and developed further throughout the present research.

1.6 Nonlinear Aeroelasticity: Concepts and Practical Examples

As the limitations of classical linear aeroelastic theories became increasingly apparent, researchers progressively turned their attention towards nonlinear aeroelasticity. Nonlinear aeroelasticity explicitly addresses scenarios wherein structural deformations become large, aerodynamic forces exhibit nonlinear characteristics, or transient dynamic behaviors significantly affect structural response. Unlike linear methods, nonlinear analysis captures realistic aeroelastic behaviors such as large structural displacements, limit cycle oscillations (LCOs), and complex transient dynamics. Understanding and accurately predicting these phenomena are critical for modern aircraft design, especially given the contemporary emphasis on lightweight materials, high flexibility, and operation in challenging flight regimes [7, 23, 14]. One of the central aspects distinguishing nonlinear aeroelasticity from its linear counterpart is geometric nonlinearity. In high-aspect-ratio wings and slender structures, structural deflections can become large enough to induce significant changes in aerodynamic load distributions, which further affect structural deformation. This nonlinear coupling can dramatically alter structural stiffness, mode shapes, and frequencies, fundamentally influencing the aeroelastic response. For example, wing bending and torsion modes can interact nonlinearly at large deflections, modifying aerodynamic stability characteristics in ways linear theories cannot predict. Such effects are particularly pronounced in modern composite wings, whose lightweight and anisotropic properties significantly contribute to geometric nonlinearities during flight operations [8, 24, 3]. Another critical source of nonlinearities arises from aerodynamic phenomena themselves. At high subsonic and transonic flight regimes, aerodynamic forces no longer vary linearly with structural deformation or angle of attack due to phenomena such as shock-induced separation, vortex shedding, and boundary-layer transition. These nonlinear aerodynamic effects significantly influence aeroelastic stability and structural response. For example, at transonic speeds, the formation

and migration of shock waves along an aircraft wing result in highly nonlinear pressure distributions that can induce abrupt changes in structural loading, destabilizing previously stable modes or causing new modes to emerge unexpectedly. Such behaviors necessitate nonlinear aerodynamic modeling approaches that accurately capture shock-induced effects and their coupling with structural deformations [13, 22, 20]. The phenomenon of limit cycle oscillations (LCOs) represents a quintessential example of nonlinear aeroelastic behavior. Unlike classical flutter, characterized by unbounded structural oscillation amplitudes, LCOs stabilize at finite amplitudes due to nonlinear aerodynamic and structural damping effects. Such oscillations result from a delicate energy balance, wherein nonlinear aerodynamic forces and structural stiffness modifications stabilize vibrations at particular amplitude levels. For instance, flexible wings of high-performance unmanned aerial vehicles (UAVs) often exhibit LCOs under certain flight conditions. In these scenarios, the structural deflections become sufficiently large to alter aerodynamic loading distributions, producing stabilizing nonlinear damping that prevents oscillation amplitudes from growing indefinitely [23, 14, 25]. A practical example of LCOs was observed explicitly in flight tests and experimental studies of military aircraft carrying external stores or weapons pods. In such configurations, external stores significantly alter aerodynamic loading, leading to nonlinear aeroelastic interactions. Experimental results have documented sustained, finite-amplitude oscillations of wings and weapon stores, demonstrating clear nonlinear aeroelastic responses. Accurate prediction of these behaviors is critical, as sustained oscillations, even at finite amplitudes, can induce fatigue damage or degrade structural integrity over extended operational periods. Such phenomena require explicitly nonlinear time-domain analysis methodologies, as classical frequency-domain linear approaches fail to capture amplitude-dependent stability characteristics [25, 11]. The complexity and critical importance of nonlinear aeroelastic behaviors have motivated the development and extensive use of computational aeroelastic methods explicitly tailored to handle these phenomena. Modern computational techniques, typically employing nonlinear time-domain simulations, accurately represent large structural deformations, nonlinear aerodynamic loading distributions, and transient dynamic behaviors. Numerical methods such as the Unsteady Vortex Lattice Method (UVLM), Computational Fluid Dynamics (CFD), and Finite Element Method (FEM) have become indispensable tools for analyzing nonlinear

aeroelastic phenomena. These methodologies explicitly account for nonlinear aerodynamic effects, geometric nonlinearities, and complex fluid-structure interactions (FSI), providing accurate predictions necessary for contemporary aircraft design and safety assessments [13, 26, 20]. Practical applications of nonlinear computational aeroelastic analyses are widespread in modern aerospace research and development. For instance, recent studies involving high-aspect-ratio UAV wings have employed coupled UVLM-FEM simulations to investigate nonlinear aeroelastic behaviors explicitly. These simulations accurately predict LCO amplitudes, flutter boundaries, and structural response patterns under realistic operational scenarios, including gust encounters, abrupt maneuvers, and varying payload configurations. Results obtained from such studies provide crucial guidance for designing wings and structures resilient to nonlinear aeroelastic instabilities, thus significantly enhancing flight safety, structural durability, and operational reliability [26, 12, 14]. Moreover, explicit computational analyses have played critical roles in the aeroelastic certification processes of modern aircraft. Regulatory agencies explicitly require accurate demonstration of aeroelastic stability throughout aircraft operating envelopes. Nonlinear computational aeroelastic simulations have proven indispensable in satisfying these certification requirements, particularly for innovative aircraft designs involving novel structural configurations, lightweight composite materials, and unconventional aerodynamic layouts. Consequently, nonlinear aeroelastic methodologies have transitioned from theoretical research tools into essential components of industry-standard aeroelastic design, validation, and certification processes [15, 16, 11]. In summary, nonlinear aeroelastic phenomena explicitly represent critical design considerations in contemporary aerospace engineering practice. Nonlinear structural and aerodynamic effects significantly influence aeroelastic stability, structural response patterns, and overall flight safety. Addressing these phenomena requires advanced computational methodologies explicitly tailored to capture large structural deflections, nonlinear aerodynamic interactions, and transient dynamic behaviors accurately. This thesis explicitly addresses these critical aeroelastic challenges through advanced computational modeling, providing aerospace engineers with reliable predictive tools to ensure the structural integrity, operational safety, and superior flight performance of modern aircraft configurations.

1.7 Limit Cycle Oscillations (LCOs): Mechanisms and Implications

Among the various nonlinear aeroelastic phenomena encountered in aerospace engineering, Limit Cycle Oscillations (LCOs) occupy a unique and particularly significant position. Unlike classical flutter, where structural oscillations grow unbounded and lead to catastrophic failure, LCOs are characterized by sustained, finite-amplitude oscillations resulting from a nonlinear balance between aerodynamic forces, structural stiffness, and damping. These oscillations are typically self-sustaining, maintaining consistent amplitudes and frequencies over prolonged periods, presenting distinctive challenges and opportunities in modern aircraft design and operational practices [23, 25, 14]. Mechanistically, LCOs emerge due to the nonlinear interplay between aerodynamic and structural forces. Structural nonlinearity, arising primarily from geometric effects due to large structural deformations or material nonlinearities, modifies structural stiffness and mode shapes as oscillation amplitudes increase. Concurrently, aerodynamic nonlinearities, such as flow separation, vortex shedding, or shock-wave movement, significantly alter aerodynamic loading distributions and their interactions with the structural response. When the structure's damping characteristics and the nonlinear aerodynamic energy input reach equilibrium, structural oscillations no longer grow exponentially. Instead, they stabilize at specific amplitude levels, resulting in the distinctively finite, persistent oscillatory behavior characteristic of LCOs [23, 11, 24]. The occurrence of LCOs has been observed in diverse aircraft configurations, from military fighter jets to civilian commercial aircraft and lightweight unmanned aerial vehicles (UAVs). A notable example involves modern fighter aircraft configurations equipped with external stores (fuel tanks, missiles, or sensor pods). These external payloads significantly alter aerodynamic loading and structural stiffness distributions, leading to pronounced nonlinear aeroelastic interactions. During flight tests and operational deployments, such aircraft have demonstrated sustained oscillations at finite amplitudes, distinctly characteristic of LCO phenomena. While these oscillations do not directly result in immediate catastrophic failure, prolonged exposure can cause cumulative fatigue damage, structural degradation, reduced operational life, and potentially impaired aircraft control and maneuverability [25, 20]. Similarly, high-aspect-ratio wings used in modern UAVs and high-performance sailplanes often exhibit LCO behavior, primarily due to their intrinsic

structural flexibility and low structural damping. In such lightweight and highly flexible structures, even moderate aerodynamic loading can cause significant structural deformation, altering aerodynamic force distributions nonlinearly and stabilizing oscillations at finite amplitudes. These sustained oscillations affect the aircraft's aerodynamic efficiency, structural durability, and operational capabilities, requiring careful prediction, analysis, and management within the design process. Understanding and accurately predicting these oscillations is particularly crucial for UAV missions involving long-duration flights, precision maneuvers, and payload deployments, where stable structural behavior is essential for mission success [26, 12]. The accurate prediction and understanding of LCO phenomena demand sophisticated nonlinear computational methodologies. Traditional linear aeroelastic theories, by their inherent nature, fail to capture the amplitude-dependent damping and nonlinear interactions essential to the formation and stabilization of LCOs. Consequently, contemporary analyses extensively employ nonlinear time-domain simulations explicitly capable of capturing the intricate nonlinear interplay of aerodynamic, structural, and inertial forces. Computational methodologies, including coupled Computational Fluid Dynamics (CFD) with Finite Element Method (FEM) structural analyses or Unsteady Vortex Lattice Method (UVLM)-based aerodynamic models integrated with nonlinear structural modeling, have demonstrated considerable accuracy in predicting LCO amplitudes, frequencies, and structural response patterns observed experimentally and in-flight tests [13, 11, 14]. Practical implications of LCOs extend beyond structural fatigue and operational safety concerns. In some circumstances, LCO phenomena can provide beneficial design insights. For instance, controlled LCO behavior may allow designers to reduce structural weight by explicitly accepting finite-amplitude oscillations within specific operational limits. This approach can enhance aircraft performance, fuel efficiency, and payload capabilities, provided the LCO amplitudes remain within structurally safe and operationally manageable ranges. Such beneficial exploitation of LCO phenomena necessitates precise computational modeling and experimental validation, ensuring oscillations remain predictable, controllable, and within structural fatigue limits [24, 23]. Moreover, LCO phenomena provide critical opportunities for researchers and engineers to study nonlinear structural dynamics and fluid-structure interactions (FSI) in realistic aerospace environments. Detailed analyses of LCO mechanisms, employing high-fidelity numerical simulations

coupled with targeted experimental studies, significantly enhance the fundamental understanding of nonlinear aeroelastic behavior. These studies have led to critical advances in analytical, computational, and experimental aeroelastic methodologies, substantially improving the predictive capabilities required for contemporary aircraft design, validation, and certification processes [13, 20, 26]. In modern aerospace certification practices, accurate identification and analysis of LCO phenomena constitute essential regulatory requirements. Regulatory authorities, including the Federal Aviation Administration (FAA) and European Union Aviation Safety Agency (EASA), explicitly require demonstrating aeroelastic stability, including LCO behavior, within the certified aircraft flight envelope. Advanced computational aeroelastic analyses, incorporating nonlinear aerodynamic and structural effects, have become integral to satisfying these regulatory requirements, ensuring aircraft designs meet stringent safety and operational standards under realistic flight conditions [13]. In conclusion, Limit Cycle Oscillations represent a critical class of nonlinear aeroelastic phenomena, uniquely characterized by stable, finite-amplitude oscillations sustained by nonlinear aerodynamic and structural interactions. The presence of LCOs in contemporary aerospace structures poses distinct challenges and opportunities, emphasizing the necessity of sophisticated computational modeling methodologies explicitly tailored to nonlinear aeroelastic analyses. This thesis explicitly addresses these challenges by developing advanced computational aeroelastic tools, providing reliable predictive capabilities for LCO behaviors and significantly contributing to the safety, reliability, and performance optimization of modern aircraft designs.

1.8 Computational Aeroelasticity and Fluid-Structure Interaction (FSI)

With the rapid advancement of computational technologies and numerical analysis methods, computational aeroelasticity has emerged as an indispensable component of modern aerospace engineering. Computational aeroelasticity explicitly addresses the complexities of aeroelastic phenomena by integrating advanced aerodynamic and structural models through robust fluid-structure interaction (FSI) methodologies. By numerically solving coupled equations governing aerodynamic flows and structural dynamics simultaneously, these computational approaches enable realistic and accu-

rate predictions of nonlinear aeroelastic behaviors, significantly surpassing the limitations inherent in classical analytical or frequency-domain linear theories [13, 11, 8]. The fundamental concept underlying computational aeroelasticity is the explicit coupling between aerodynamic and structural models within a unified computational framework. Aerodynamic models such as Computational Fluid Dynamics (CFD) or the Unsteady Vortex Lattice Method (UVLM) explicitly calculate aerodynamic loads, pressures, and forces acting on the structure. Simultaneously, structural analysis methods, predominantly employing the Finite Element Method (FEM), explicitly determine structural displacements, stresses, and dynamic response characteristics. At each computational time step, aerodynamic forces calculated from the aerodynamic solver explicitly drive structural deformation, which in turn modifies aerodynamic boundary conditions, creating a continuous feedback loop characteristic of fluid-structure interactions [7, 26, 20]. Among various aerodynamic modeling approaches in computational aeroelasticity, Computational Fluid Dynamics (CFD) provides the highest fidelity. CFD explicitly solves the Navier–Stokes equations governing fluid flow around complex geometries, capturing nonlinear aerodynamic phenomena such as shock waves, boundary-layer separations, vortical flows, and transient aerodynamic loading. CFD simulations can resolve detailed flow structures, pressure distributions, and transient aerodynamic phenomena with remarkable accuracy, particularly essential for high-speed or transonic aeroelastic analyses. However, CFD simulations typically require significant computational resources, necessitating efficient numerical strategies or reduced-order models when applied in coupled FSI analyses [13, 12, 11]. In contrast, the Unsteady Vortex Lattice Method (UVLM) offers computational efficiency with reasonable accuracy for aerodynamic analyses within subsonic and low-transonic regimes. UVLM explicitly models lifting surfaces as discrete vortex elements distributed over panel discretizations, calculating aerodynamic loads through induced velocities and circulation strengths governed by the Biot–Savart law. Although UVLM does not explicitly capture viscous or strongly nonlinear compressibility effects inherent in transonic or supersonic flows, its computational efficiency makes it particularly suitable for preliminary aeroelastic design, optimization studies, and analyses involving large parametric variations. UVLM's computational speed also facilitates extended time-domain simulations necessary for transient aeroelastic studies and LCO analyses, making it highly advan-

tageous for practical aeroelastic analyses of flexible aircraft wings and UAV configurations [26, 2, 3]. Structural analyses within computational aeroelasticity predominantly employ the Finite Element Method (FEM), renowned for its versatility, accuracy, and widespread acceptance within aerospace structural engineering. FEM explicitly discretizes the aircraft structure into interconnected finite elements, accurately representing structural stiffness, mass distribution, and damping characteristics. The structural solver explicitly computes structural displacements, natural frequencies, mode shapes, and stress distributions under aerodynamic loading, accommodating geometric nonlinearities arising from large deflections, material nonlinearities, and complex boundary conditions. The explicit coupling of FEM structural analyses with CFD or UVLM aerodynamic models provides a powerful computational framework for accurately capturing nonlinear aeroelastic interactions in contemporary aerospace configurations [8, 13, 11]. Fluid-Structure Interaction (FSI) techniques form the cornerstone of computational aeroelasticity, explicitly enabling rigorous numerical coupling between aerodynamic and structural solvers. In an FSI framework, aerodynamic loads from CFD or UVLM simulations explicitly provide external forcing conditions for the structural FEM solver. The resulting structural displacements explicitly update aerodynamic boundary conditions in the subsequent aerodynamic simulation step. This iterative computational process explicitly continues throughout the numerical simulation, ensuring consistency between aerodynamic loading and structural response at each computational step, thus accurately capturing the inherent dynamic interactions within aeroelastic phenomena. Computationally, FSI coupling can be realized using tightly coupled methods (fully coupled solvers) or loosely coupled approaches (explicit exchange of data between aerodynamic and structural solvers), depending on the computational resources and fidelity requirements of the analysis [14, 20, 13]. Practical applications of computational aeroelasticity and FSI analyses span a broad spectrum of aerospace research, design, and certification processes. Explicitly, computational aeroelastic methods play critical roles in predicting flutter boundaries, limit cycle oscillation behaviors, transient responses to gust encounters, and aeroelastic effects of external payloads or structural modifications. For example, modern UAV designs extensively utilize coupled UVLM-FEM analyses to investigate structural flexibility effects on flight dynamics, aerodynamic efficiency, and payload integration. Similarly, military aircraft configurations

rely on detailed CFD-FEM coupled simulations to ensure aeroelastic stability during high-speed maneuvers, weapon-store integration, and transonic operations. The outcomes from these analyses explicitly inform critical design decisions, optimize structural configurations, and significantly enhance flight safety, reliability, and performance [26, 11, 12]. Moreover, regulatory certification processes increasingly mandate comprehensive computational aeroelastic analyses explicitly employing coupled FSI methodologies. Regulatory bodies such as the FAA and EASA explicitly require demonstration of aeroelastic stability, explicitly validated through computational simulations complemented by experimental testing. Computational aeroelastic analyses explicitly serve as indispensable tools to satisfy these regulatory requirements, ensuring aircraft meet stringent safety and operational standards under realistic aeroelastic conditions encountered throughout their operational envelopes [15, 16, 13]. In summary, computational aeroelasticity and fluid-structure interaction methodologies explicitly provide powerful and versatile analytical tools essential for contemporary aerospace engineering practice. The accurate and efficient prediction of aeroelastic phenomena achieved through these computational approaches significantly enhances structural safety, operational reliability, and performance optimization of modern aircraft configurations. This thesis explicitly contributes to advancing computational aeroelastic methodologies by developing and validating a robust computational tool integrating UVLM aerodynamic modeling and FEM structural analyses, addressing contemporary aeroelastic challenges explicitly relevant to flexible, high-performance aerospace systems.

1.9 Current State-of-the-Art and Research Gaps

Contemporary aeroelastic research has advanced significantly, driven by the increased complexity of aircraft designs and the availability of powerful computational resources. Current state-of-the-art aeroelastic analyses utilize sophisticated computational fluid dynamics (CFD) coupled with advanced structural modeling techniques, typically the Finite Element Method (FEM), integrated within robust fluid-structure interaction (FSI) frameworks. These advanced methodologies enable highly accurate predictions of complex aeroelastic behaviors, including flutter, transient dynamic re-

sponses, and nonlinear structural interactions, surpassing classical linear aeroelastic analysis methods significantly [13, 11, 14]. Despite remarkable advances, several critical gaps and limitations persist within current computational aeroelastic methodologies, explicitly highlighting opportunities for research and improvement. Addressing these gaps is crucial to ensure accurate and reliable aeroelastic predictions, especially as aircraft designs continue evolving towards higher flexibility, lighter structural weight, and more complex aerodynamic configurations. A significant current challenge involves accurately and efficiently modeling nonlinear aeroelastic phenomena at transonic and supersonic flight conditions. The presence of nonlinear aerodynamic effects, including shock-induced separation, vortex formation, and complex boundary-layer interactions, significantly complicates aeroelastic predictions. While CFD-based methods provide high accuracy, their computational costs remain considerable, limiting their use in large-scale parametric studies, preliminary design optimization, or extensive uncertainty analyses. Consequently, there is a clear need for efficient reduced-order models (ROMs) that accurately capture key nonlinear aerodynamic features with significantly reduced computational demands, facilitating broader applicability in practical aeroelastic analyses [12, 20, 27]. In addition, accurately predicting non-linear structural responses in flexible aerospace structures remains a challenge. High-aspect-ratio wings, composite materials, and lightweight structural components often exhibit geometric and material nonlinearities under realistic aerodynamic loading. Traditional linear structural models and simplified nonlinear approximations frequently prove inadequate for capturing these nonlinear structural effects accurately. Research efforts aimed at integrating advanced nonlinear structural models within computational aeroelastic frameworks, particularly capturing geometric nonlinearities and large deformation effects efficiently and accurately, represent critical needs within contemporary aeroelastic research [8, 24]. Another important research gap relates to transient aeroelastic phenomena arising from gust encounters, abrupt maneuvers, or rapid control-surface deflections. Accurately simulating transient aeroelastic responses demands computational methods capable of capturing highly dynamic, nonlinear aerodynamic-structural interactions efficiently. Existing high-fidelity CFD-FEM coupled analyses, while accurate, are often computationally prohibitive for extensive transient simulations or probabilistic assessments required in aircraft certification processes. Thus, the development of efficient com-

putational approaches, explicitly capturing transient aeroelastic phenomena, and enabling rapid assessments of aeroelastic stability and dynamic responses remains a critical and largely unresolved research challenge [20, 13, 26]. Moreover, uncertainties associated with material properties, manufacturing tolerances, aerodynamic modeling assumptions, and operational conditions further complicate aeroelastic predictions. Traditional deterministic analyses typically neglect these uncertainties, potentially resulting in overly optimistic or inaccurate stability assessments. Recent research increasingly recognizes the importance of uncertainty quantification (UQ) within computational aeroelastic frameworks. Integrating robust UQ methodologies explicitly within computational aeroelastic analyses, facilitating probabilistic assessments of stability margins, structural fatigue risks, and operational reliability, represents a crucial and emerging research direction within contemporary aeroelasticity [27, 28]. Furthermore, integrating active and passive control strategies within computational aeroelastic analyses represents a promising and active research area. Advances in materials technology, sensors, and actuators enable practical implementation of adaptive structural components and active aeroelastic control systems explicitly designed to mitigate undesirable aeroelastic behaviors such as flutter, or transient responses. Computational aeroelastic methodologies explicitly incorporating control algorithms, adaptive structures, and real-time feedback mechanisms remain underdeveloped, presenting clear opportunities for significant research advancements explicitly benefiting modern aircraft design, safety, and performance optimization [25, 14, 20]. In response to these identified research gaps, this thesis explicitly aims to address critical aspects of nonlinear computational aeroelastic modeling explicitly. Specifically, the thesis develops and validates a robust computational aeroelastic solver explicitly coupling aerodynamic analyses based on the Unsteady Vortex Lattice Method (UVLM) with advanced nonlinear structural models using the Finite Element Method (FEM). The developed solver explicitly targets efficient and accurate prediction of flutter boundaries, limit cycle oscillations, and nonlinear transient responses, specifically addressing computational efficiency concerns, accuracy of nonlinear aerodynamic-structural interactions, and practical applicability within contemporary aerospace engineering practice. In conclusion, contemporary aeroelastic research has significantly advanced, providing sophisticated computational methodologies explicitly capable of accurately predicting complex aeroelastic phenomena. Nevertheless, several critical research

gaps persist, particularly concerning efficient nonlinear modeling approaches, accurate prediction of limit cycle oscillations and transient behaviors, uncertainty quantification, and integration of advanced control methodologies. Addressing these gaps explicitly represents crucial research opportunities that this thesis explicitly aims to contribute towards, providing reliable, efficient, and accurate computational aeroelastic tools essential for the design, certification, and operational safety of modern aircraft configurations.

1.10 Motivation and Objectives of the Thesis

Based on the comprehensive review of historical developments, theoretical advancements, and contemporary research gaps identified in previous sections, the central objectives of this thesis explicitly address critical challenges in computational aeroelastic analysis, particularly concerning nonlinear flutter. The aim of this research is to develop, implement, and validate an efficient and robust in-house computational aeroelastic solver explicitly designed to capture nonlinear, unsteady aeroelastic behaviors, ensuring accuracy, computational efficiency, and practical applicability to the design of aerospace systems.

The detailed research objectives of this thesis are summarized as follows:

1. **Development of an In-House Computational Aeroelastic Solver:** To develop an efficient, robust, and versatile aeroelastic solver explicitly based on the coupling of the Unsteady Vortex Lattice Method (UVLM) for aerodynamic modeling and the Finite Element Method (FEM) for structural analysis.

   The developed solver aims to capture nonlinear, unsteady aerodynamic effects, large structural deformations, and transient aeroelastic phenomena within an efficient computational framework, overcoming the limitations of classical linear methods.

2. **Verification and Validation of the Developed Solver:** To rigorously verify the accuracy and numerical stability of the solver against established analytical solutions, classical aeroelastic benchmarks, and experimental results from the available literature.

The selected validation cases include classical flutter predictions, known limit cycle oscillations, and transient aeroelastic responses to ensure reliability and robustness in practical aeroelastic applications.

3. **Comprehensive Analysis of Flutter and Limit Cycle Oscillations:** To systematically investigate nonlinear aeroelastic phenomena, explicitly focusing on the accurate prediction of flutter onset conditions, stable limit cycle oscillation amplitudes, and transient dynamic aeroelastic behaviors under realistic flight conditions.

   The analysis explicitly considers variations in aerodynamic parameters, structural properties, and operational scenarios to capture comprehensive aeroelastic stability characteristics.

4. **Demonstration of Computational Efficiency and Practical Applicability:** To demonstrate the computational efficiency, practicality, and effectiveness of the developed solver explicitly through extensive parametric studies, comparative analyses, and realistic case studies.

   The practical applications selected include test cases establishing the solver's suitability for preliminary design evaluations, parametric optimization studies, and robust aeroelastic assessments within industrial aerospace applications.

Through explicit fulfillment of these objectives, the thesis aims to provide significant contributions to current aeroelastic research, specifically addressing critical computational modeling challenges, practical limitations in aeroelastic predictions, and advancing the state-of-the-art in nonlinear, unsteady aeroelastic analyses relevant to modern flexible aerospace systems.

In summary, this thesis addresses computational challenges in aeroelastic research, explicitly focusing on nonlinear flutter, limit cycle oscillations, and transient dynamic phenomena. By developing and validating an advanced computational aeroelastic solver based on coupling UVLM aerodynamic modeling with FEM structural analyses, the research contributes robust, fast and efficient analytical tools essential for accurately predicting aeroelastic behaviors during early design phases of modern, flexible aircraft configurations. The outcomes of this research explicitly aim to enhance aeroelastic prediction capabilities, improve structural safety and reliability, and

facilitate practical aeroelastic design optimization processes within the aerospace industry.

1.11 Outline of the Thesis

The thesis is explicitly structured into five chapters, providing a coherent and systematic presentation of the research methodology, numerical developments, comprehensive validation studies, and practical aeroelastic analysis results.

A brief outline explicitly describing each chapter is provided below:

- **Chapter 1 – Introduction:** Provides a comprehensive introduction to aeroelasticity, explicitly covering historical developments, theoretical foundations, linear and nonlinear aeroelastic theories, computational methodologies, current state-of-the-art, critical research gaps, and clearly defined research objectives.

  The chapter explicitly establishes the context, motivation, and fundamental background necessary for understanding the subsequent research conducted in this thesis.

- **Chapter 2 – Computational Aeroelastic Methodology:** Presents a detailed description of the computational methodologies used and developed within this research, focusing on the mathematical formulations, theoretical derivations, numerical implementation, and practical coupling approaches between the Unsteady Vortex Lattice Method (UVLM) aerodynamic solver and Finite Element Method (FEM) structural solver.

  The chapter describes the newly developed in-house UVLM/FEM solver, called as AeroWing, and emphasizes the solver efficiency, nonlinear modeling techniques, and rigorous implementation details crucial for accurate aeroelastic predictions.

- **Chapter 3 – Verification and Validation Studies:** Describes comprehensive verification and validation efforts explicitly conducted to ensure the accuracy, stability, and robustness of the developed computational aeroelastic solver.

The explicit comparisons against analytical solutions such as Theodorsen's Function, established aeroelastic benchmarks, and experimental results from published literature explicitly are presented in this chapter to demonstrate the solver's accuracy, reliability, and suitability for nonlinear aeroelastic analyses, including flutter predictions and limit cycle oscillations.

- **Chapter 4 – Nonlinear Aeroelastic Simulations and Results:** Presents detailed computational studies explicitly conducted using the validated solver, systematically analyzing nonlinear aeroelastic phenomena, including flutter boundaries, transient dynamic responses, and parameter sensitivity analyses.

  The realistic test case studies are selected and presented to explicitly demonstrate solver applicability, providing critical insights into nonlinear aeroelastic interactions, stability margins, and practical design considerations for contemporary aerospace systems.

- **Chapter 5 – Conclusions and Future Work:** Summarizes the key findings, contributions, and conclusions explicitly derived from the research conducted.

  The chapter explicitly discusses the solver's achievements and practical implications for aerospace design and certification. Recommendations and directions are provided for future research efforts to further develop computational aeroelastic methodologies and expand their scope of application.

CHAPTER 2

METHODOLOGY

In this thesis, a computational aeroelastic analysis tool is developed which includes the Unsteady Vortex Lattice Method (UVLM) with free wake for aerodynamic load calculations and the Finite Element Modeling (FEM) for dynamic motion/deformation calculations. The computational aeroelastic analysis tool integrates the structural dynamics with unsteady aerodynamic forces to predict the flutter behavior. The iterative coupling approach ensures the accurate representation of the interactions between the structural motion and the wake dynamics, forming a robust tool for aeroelastic analysis.

Analyzing aeroelastic phenomena such as flutter is complex and requires advanced computational tools that accurately model nonlinear interactions between structural dynamics and aerodynamic forces. Traditional linear aeroelastic methods often miss critical nonlinear behaviors, making it essential to perform simulations in the time domain. In this research, an integrated computational method that couples the Unsteady Vortex Lattice Method (UVLM) for aerodynamic analysis with the Finite Element Method (FEM) for structural response analysis is used. This combined approach allows for a detailed and realistic representation of nonlinear aeroelastic effects encountered in modern aerospace structures.

The methodology developed in this study emphasizes the interaction between aerodynamics and structural dynamics. At each time step of the simulation, aerodynamic forces obtained through UVLM calculations are applied directly to the structural model. These forces cause structural deformations, which in turn affect the aerodynamic panel positions and, consequently, the aerodynamic forces in subsequent steps. This iterative process ensures a realistic coupling between aerodynamic and

structural responses.

A significant advantage of the approach used in this study is the shared discretization between aerodynamic and structural domains. Specifically, the aerodynamic panels used in the UVLM model coincide exactly with the structural finite elements used in the FEM model. This eliminates the need for interpolation or mapping between different meshes, greatly improving both numerical stability and computational accuracy.

The computational workflow employed follows three main steps:

1. **Aerodynamic Analysis**: Aerodynamic surfaces are discretized using vortex lattice panels. Circulation strengths are determined by enforcing boundary conditions at panel control points. Wake dynamics are explicitly simulated to track vortex shedding, a crucial component for accurate transient aerodynamic analysis.

2. **Structural Dynamics Analysis**: FEM is used to calculate the structural responses. This involves discretizing the surface into plate elements, assembling the mass and stiffness matrices based on standard plate theories, and applying boundary conditions such as clamped or pinned edges.

3. **Coupled Aero-Structural Interaction**: The structural displacements from the FEM analysis update aerodynamic panel positions for the UVLM calculations, and the resulting aerodynamic loads again feed back into structural analysis. This iterative loop continues at each timestep, ensuring accurate modeling of fluid-structure interactions.

Non-circulatory aerodynamic effects, including added mass due to structural acceleration, are explicitly considered in the simulation. These effects significantly impact the transient aerodynamic loading, particularly during rapid structural movements or sudden gust interactions.

Additionally, to realistically represent structural conditions, plunge and pitch dynamics are explicitly modeled. Linear and torsional springs at specific structural nodes

simulate realistic stiffness and boundary conditions. These details enable the precise simulation and analysis of key aeroelastic phenomena flutter onset.

The computational framework developed is implemented in an in-house solver, AeroWing, based on coupled UVLM/FEM method. Its modular structure provides flexibility in adjusting model parameters, computational strategies, and incorporating additional physical phenomena. This adaptability ensures that the methodology can accommodate various aeroelastic scenarios and be extended to future research efforts.

2.1 Methodology for Aerodynamic Analysis

In this research, the Unsteady Vortex Lattice Method (UVLM) is used to accurately model aerodynamic forces in aeroelastic scenarios. UVLM is particularly effective for investigating flexible lifting surfaces under conditions where airflow varies over time.

2.1.1 Unsteady Vortex Lattice Method (UVLM)

Unsteady Vortex Lattice Method (UVLM) is based on potential flow theory and relies on several simplifying assumptions, such as incompressible, inviscid, and irrotational flow, making it computationally efficient yet sufficiently accurate for capturing crucial aerodynamic effects [2, 29, 30].

To streamline the aerodynamic analysis, UVLM adopts the following primary assumptions:

- **Incompressible Flow:** The flow is assumed incompressible, satisfying:

$$\nabla \cdot \mathbf{v} = 0 \tag{2.1}$$

  where, $\mathbf{v}$ is the velocity field.

- **Irrotational Flow:** The flow is irrotational in the domain, meaning:

$$\nabla \times \mathbf{v} = 0 \tag{2.2}$$

  which implies the absence of vorticity in the field [31].

- **Inviscid Flow:** Viscous effects are negligible, simplifying the governing equations [2].

- **Thin Airfoil Approximation:** The geometry of the airfoil is assumed thin, allowing for linearized flow calculations [19].

Under these conditions, the flow field velocity can be described by using a velocity potential function ϕ, which required the solution of the Laplace equation as the governing equation:

$$\nabla^2 \phi = 0 \tag{2.3}$$

2.1.2 UVLM Panel Discretization

In UVLM, the wing planform and wake are discretized into N panels as shown in Figures 2.1 and 2.2. Each panel on the wing is represented by a bound vortex, and free vortices are shed from the trailing edge to form the wake. The circulation strength (Γ) of these vortices determines the induced velocity and aerodynamic forces [29].

Each vortex panel contributes to the induced velocity field Figure 2.1. Using the Biot-Savart law, the velocity induced at a point $\mathbf{r}$ by a vortex filament is:

$$\mathbf{v}_{\text{ind}}(\mathbf{r}) = \frac{\Gamma}{4\pi} \int \frac{(\mathbf{r} - \mathbf{r}') \times \mathbf{d}\ell}{\|\mathbf{r} - \mathbf{r}'\|^3} \tag{2.4}$$

where, Γ is circulation strength of the vortex, $\mathbf{r}$ is position vector of observation point, $\mathbf{r}'$ is position vector of the vortex filament, $\mathbf{d}\ell$ is differential length along the vortex filament [31].

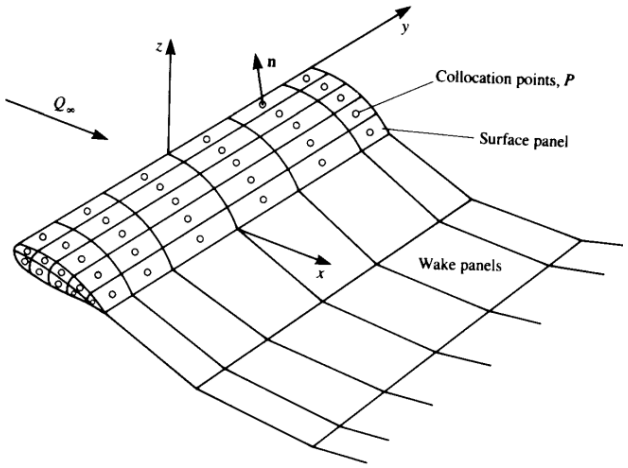

Figure 2.1: Representation of an aeroelastic wing model showing surface panels, wake panels, and collocation points for aerodynamic force calculations, adapted from [2].

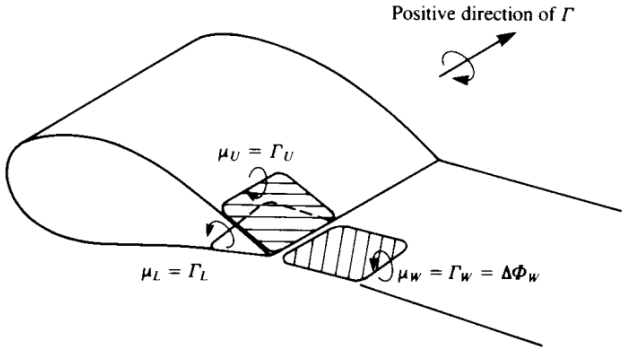

Figure 2.2: Kutta condition usage, adapted from [2].

2.1.3 Governing Equations and Boundary Conditions

Circulation strengths around each aerodynamic panel are computed by enforcing a boundary condition that ensures no airflow penetrates through the surface. This boundary condition results in a set of linear algebraic equations that must be solved at every simulation step:

$$\sum_{j=1}^{N} A_{ij}\Gamma_j = \left(\mathbf{V}_\infty + \mathbf{V}_{\text{body}} + \mathbf{V}_{\text{wake}}\right)_i \cdot \mathbf{n}_i \tag{2.5}$$

To uniquely solve for ϕ, boundary conditions are applied:

1. **Kinematic Boundary Condition:** The velocity of the flow normal to the airfoil surface must equal the surface velocity:

$$\frac{\partial \phi}{\partial n} = \mathbf{v}_{\text{body}} \cdot \mathbf{n} \tag{2.6}$$

   where, $\mathbf{n}$ is the normal vector to the surface [32].

2. **Kutta Condition:** At the trailing edge, the flow leaves the surface smoothly Figure 2.2, ensuring finite velocities [2].

2.1.4 Numerical Solution Methodology: Solving for Γ

The vortex strengths Γ_i for all panels are calculated by enforcing the kinematic boundary condition (Eq. 2.6) at the collocation points. This yields a system of linear equations:

$$\mathbf{A\Gamma} = \mathbf{b} \tag{2.7}$$

$$\begin{bmatrix} a_{11} & a_{12} & a_{13} & \cdots & a_{1N} & a_{1W} \\ a_{21} & a_{22} & a_{23} & \cdots & a_{2N} & a_{2W} \\ a_{31} & a_{32} & a_{33} & \cdots & a_{3N} & a_{3W} \\ \vdots & \vdots & \vdots & \ddots & \vdots & \vdots \\ a_{N1} & a_{N2} & a_{N3} & \cdots & a_{NN} & a_{NW} \\ 1 & 1 & 1 & \cdots & 1 & 1 \end{bmatrix} \begin{bmatrix} \Gamma_1 \\ \Gamma_2 \\ \Gamma_3 \\ \vdots \\ \Gamma_N \\ \Gamma_{Wi} \end{bmatrix} = \begin{bmatrix} b_1 \\ b_2 \\ b_3 \\ \vdots \\ b_N \\ \Gamma(t - \Delta t) \end{bmatrix} \tag{2.8}$$

where,

- $\mathbf{A}$: Influence coefficient matrix, representing the velocity induced by each vortex at each collocation point [29],
- $\mathbf{\Gamma}$: Vector of unknown circulation strengths,
- $\mathbf{b}$: Known velocity components from the freestream and body motion [30].

By solving this system, the circulation strengths Γ_i are determined, which are then used to compute aerodynamic forces and moments. At each time increment, the size of $\mathbf{A}$, $\mathbf{\Gamma}$, and $\mathbf{b}$ increases by one, as shown in Eq. 2.8.

2.1.5 Aerodynamic Forces and Moments

Aerodynamic lift and pitching moments are calculated directly from vortex panel circulations using the Kutta-Joukowski theorem. By summing contributions from each wing vortex lattice panel, these aerodynamic forces can be determined, which subsequently interact with the structural model.

The calculated circulation strengths Γ_i represent the fundamental aerodynamic response of the airfoil to unsteady flow conditions. By incorporating wake dynamics and using the Lamb-Oseen model, UVLM captures critical phenomena such as:

- Accurate modeling of unsteady lift and pitching moment.
- Representation of wake interaction and vortex shedding.
- Prediction of aerodynamic forces under dynamic conditions [32, 11].

$$F_{\text{lift}} = \rho U \sum_{i=1}^{N} \Gamma_i \Delta x \tag{2.9}$$

where, ρ is air density, U is freestream velocity, Γ_i is circulation strength of the i-th panel, Δx is width of each panel [2].

The aerodynamic pitching moment about the elastic axis is:

$$M_{\text{pitch}} = \sum_{i=1}^{N} \Gamma_i (x_i - x_{\text{ea}}) \Delta x \tag{2.10}$$

The UVLM provides an efficient and powerful tool for analyzing unsteady aerodynamic forces. By discretizing the airfoil and wake into vortex panels and calculating circulation strengths via boundary conditions, it bridges the gap between theoretical potential flow principles and practical aeroelastic applications Fig. 2.6.

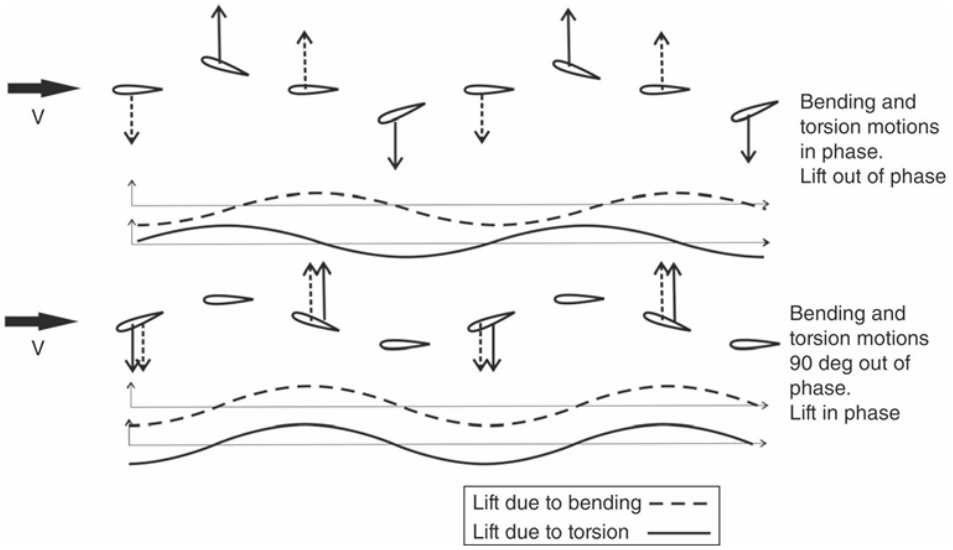

Figure 2.3: Lift components due to plunging and pitching motions [3].

2.1.6 Comparison of Vortex Core Models

Vortex core models are crucial in representing the tangential velocity distribution in vortical flows, avoiding singularities at the vortex axis and providing a more physically realistic representation of viscous effects or empirical adjustments. The Lamb–Oseen vortex is a classical solution derived from the Navier–Stokes equations for an axisymmetric vortex in a viscous fluid [33, 34], the Rankine vortex is a simpler, piecewise-defined model often used historically and in basic aerodynamic theory [31], while the Burnham–Hallock and Vatistas models introduce parameters that provide families of velocity profiles with adjustable shapes [35, 36].

Below, four models vortex core models are presented: Lamb–Oseen, Rankine, Burnham–Hallock, and Vatistas, each defining the tangential velocity v_θ as a function of radius r, circulation Γ, and core radius a.

- **Lamb-Oseen Vortex Core Model:**

  The Lamb–Oseen model [33, 34] represents a viscous vortex. It smoothly tran-

sitions from zero at the center to a maximum and then decays with radius:

$$v_\theta(r) = \frac{\Gamma}{2\pi r}\left(1 - e^{-(r^2/a^2)}\right) \tag{2.11}$$

- **Rankine Vortex Core Model:**

  The Rankine vortex [31] is a simple, piecewise model:

$$v_\theta(r) = \begin{cases} \frac{\Gamma}{2\pi a^2} r, & r \leq a \\ \frac{\Gamma}{2\pi r}, & r > a \end{cases} \tag{2.12}$$

- **Burnham–Hallock Vortex Core Model:**

  The Burnham–Hallock model [35] introduces a shape parameter m:

$$v_\theta(r) = \frac{\Gamma}{2\pi r}\left[1 - \exp\left(-(r/a)^m\right)\right] \tag{2.13}$$

- **Vatistas Vortex Core Model:**

  The Vatistas model [36] uses a parameter n:

$$v_\theta(r) = \frac{\Gamma}{2\pi a}\frac{(r/a)}{\left[1 + (r/a)^n\right]^{1/n}} \tag{2.14}$$

All four models share the circulation Γ, core radius a, radial distance r, and shape parameters m and n. Vortex core models differ in how the velocity transitions from the core region to the outer potential vortex flow as shown in Fig. 2.9. Lamb–Oseen and Vatistas can approximate realistic viscous vortices, Rankine is a simple baseline, and Burnham–Hallock provides flexibility through m.

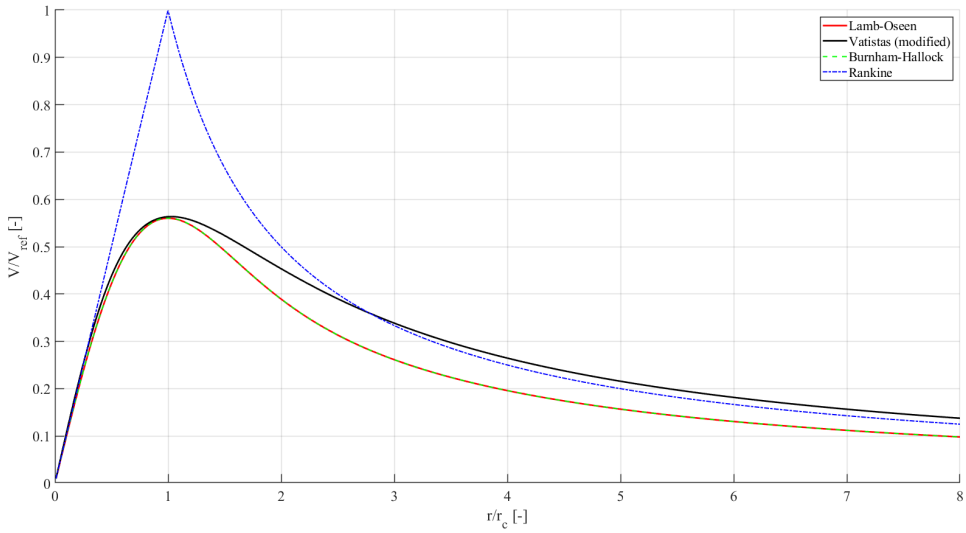

Figure 2.4: Comparison of Vortex Core Models

2.2 Methodology for Structural Analysis

For aeroelastic analyses for coupled aerodynamic/structural interactions, simple 2-D/3-D aerodynamic shapes can be represented with simplified two-degrees-of-freedom model. To model the structural dynamics involved in aeroelastic scenarios, Finite Element Method (FEM), a widely trusted computational approach in structural engineering can be used.

The Finite Element Method (FEM) divides a complex structure into smaller, manageable elements connected at nodes, allowing to analyze detailed structural behaviors under various loading conditions.

The dynamic behavior of the airfoil in plunge and pitch can be described mathematically by equations of motion derived from fundamental physics for FEM. These equations relate the structural properties of the airfoil (mass, stiffness, and damping) to the forces and moments acting on it.

The governing equations for this two-degrees-of-freedom (2-DoF) system are:

$$m\ddot{h}(t) + S_\alpha \ddot{\alpha}(t) + k_h h(t) + c_h \dot{h}(t) = \mathbf{F}_{\text{aero}}(t) \tag{2.15}$$

$$S_\alpha \ddot{h}(t) + I_e \ddot{\alpha}(t) + k_\alpha \alpha(t) + c_\alpha \dot{\alpha}(t) = \mathbf{M}_{\text{aero}}(t) \tag{2.16}$$

These equations are widely used in aeroelastic modeling, as they provide a simplified yet robust framework for analyzing airfoil dynamics [32, 37].

The structure is discretized into several finite elements, and within each element, displacements are approximated using shape functions as follows:

$$\nu_e(x,t) = \sum_{i=1}^{n_e} N_i(x) u_i(t) \tag{2.17}$$

where, $N_i(x)$ are the chosen shape functions, and $u_i(t)$ represent nodal displacements. shape functions are used to ensure continuity of both displacement and slope. For plate elements, bi-linear shape functions are commonly used, providing accurate modeling of transverse displacements and rotations.

2.2.1 Meshing

The structure is discretized into a mesh of elements, as shown in Figure 2.5. The choice of mesh density depends on the desired accuracy and computational efficiency.

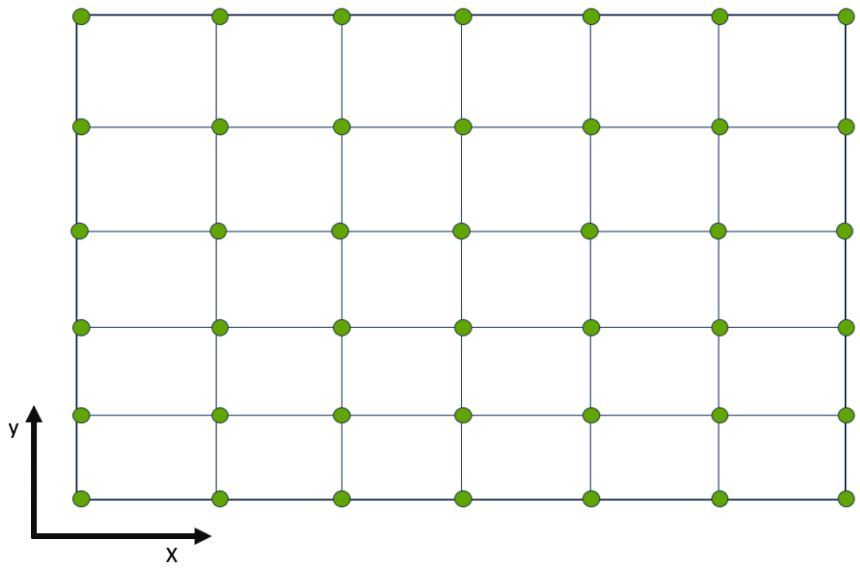

Figure 2.5: Finite element mesh of a thin rectangular plate

2.2.2 Finite Element Matrices

The element-level matrices (mass, stiffness, damping) are calculated by integrating structural properties across each element:

$$\mathbf{M}_e = [M_e] = \int_0^L \rho A N^T N \, dx \tag{2.18}$$

$$\mathbf{K}_e = [K_e] = \int_0^L EI \frac{\mathrm{d}N^T}{\mathrm{d}x} \frac{\mathrm{d}N}{\mathrm{d}x} \, dx \tag{2.19}$$

$$\mathbf{C}_e = [C_e] = \alpha[M_e] + \beta[K_e] \tag{2.20}$$

Here, ρ is the density of the material, A is the cross-sectional area, EI represents flexural rigidity, and α and β are Rayleigh damping coefficients. These element matrices are then assembled into global matrices that represent the entire structure.

2.3 Methodology for Coupled Aerodynamic/Structural Analysis

The FEM-derived structural displacements are directly linked with aerodynamic forces calculated from the UVLM model. This integrated approach ensures accurate and realistic aeroelastic simulations.

For aeroelastic analyses for coupled aerodynamic/structural interactions, simple 2-D/3-D aerodynamic shapes can be modelled with simplified two-degrees-of-freedom motions of:

- Plunge and Pitch Motion (2-D Airfoil or 3-D Plate)
- Bending and Torsion Motion (3-D Plate)

as described in the following sections.

2.3.1 Understanding Plunge and Pitch Motion in Aeroelasticity

Aeroelastic systems often involve complex interactions between the aerodynamic forces and the structural responses. To simplify the analysis and focus on the core dynamics, engineers typically examine dominant modes of motion. For a thin airfoil, these are the *plunge* (h) and *pitch* (α) motions. These two-degrees-of-freedom are sufficient to capture the primary behaviors that lead to aeroelastic instability, such as flutter [6, 8].

Because of 3-D bending and torsional deformations of a wing, its airfoil section encounters coupled plunge and pitch motions. Figure 2.6 shows the lift components due to bending and torsion motions for a wing [3]. Both motions are coupled, meaning that a change in one can influence the other. This coupling is critical to understanding the overall stability of the system [38].

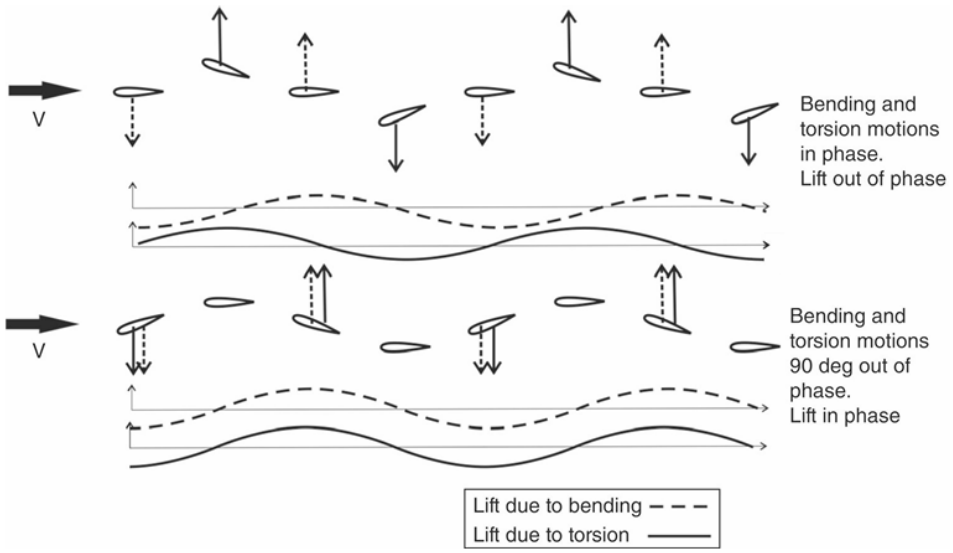

Figure 2.6: Lift components due to bending and torsion motions [3].

To understand the complex interactions, a thin airfoil can be considered and modelled which can do plunge and pitch motion as shown in Figure 2.7 under the effect of the aerodynamics loads:

- **Plunge (h)** motion represents the vertical motion of the airfoil's center of grav-

ity, moving up or down perpendicular to the freestream flow direction.

- **Pitch** (α) motion refers to the rotational motion of the airfoil about a defined axis, often the elastic axis (EA) or pitch axis.

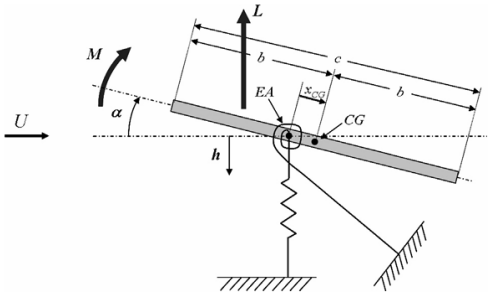

Figure 2.7: Model for plunge and pitch motion [4].

2.3.2 Equations of Motion for Plunge and Pitch

The dynamic behavior of the airfoil in plunge and pitch can be described mathematically by equations of motion derived from fundamental physics for FEM. These equations relate the structural properties of the airfoil (mass, stiffness, and damping) to the forces and moments acting on it.

The governing equations for this two-degrees-of-freedom (2-DoF) system are:

$$m\ddot{h}(t) + S_\alpha \ddot{\alpha}(t) + k_h h(t) + c_h \dot{h}(t) = \mathbf{F}_{\text{aero}}(t) \tag{2.21}$$

$$S_\alpha \ddot{h}(t) + I_e \ddot{\alpha}(t) + k_\alpha \alpha(t) + c_\alpha \dot{\alpha}(t) = \mathbf{M}_{\text{aero}}(t) \tag{2.22}$$

These equations are widely used in aeroelastic modeling, as they provide a simplified yet robust framework for analyzing airfoil dynamics [32, 37].

2.3.3 Aerodynamic and Structural Coupling

The interaction between aerodynamic forces and structural motion forms the core of the aeroelastic phenomena. The interactions are governed by two main factors:

1. **Inertial Coupling**: The structural properties of the airfoil, such as its mass and moment of inertia, result in inertial effects that couple plunge and pitch motions.

2. **Aerodynamic Coupling**: The forces and moments generated by airflow around the airfoil depend on both its vertical and angular displacements, as well as their time rates of change [39].

To better understand this coupling, the equations of motion can be expressed in matrix form:

$$\begin{bmatrix} m & S_\alpha \\ S_\alpha & I_e \end{bmatrix} \begin{bmatrix} \ddot{h}(t) \\ \ddot{\alpha}(t) \end{bmatrix} + \begin{bmatrix} c_h & 0 \\ 0 & c_\alpha \end{bmatrix} \begin{bmatrix} \dot{h}(t) \\ \dot{\alpha}(t) \end{bmatrix} + \begin{bmatrix} k_h & 0 \\ 0 & k_\alpha \end{bmatrix} \begin{bmatrix} h(t) \\ \alpha(t) \end{bmatrix} = \begin{bmatrix} \mathbf{F}_{\text{aero}}(t) \\ \mathbf{M}_{\text{aero}}(t) \end{bmatrix} \tag{2.23}$$

The matrix representation is commonly used in both theoretical and computational aeroelastic studies [40, 8].

2.3.4 Finite Element Method for Structural Dynamics

To analyze the structural behavior of thin airfoils and rectangular plates, the Finite Element Method (FEM) is employed. FEM is a robust numerical technique that discretizes the structure into smaller elements, allowing for accurate modeling of complex geometries, boundary conditions, and material properties.

The continuous governing equations of motion for the system are given by:

$$\mathbf{M}\ddot{\mathbf{u}}(t) + \mathbf{C}\dot{\mathbf{u}}(t) + \mathbf{K}\mathbf{u}(t) = \mathbf{F}(t) \tag{2.24}$$

where, M is the mass matrix, C is the damping matrix, K is the stiffness matrix, $\mathbf{u}(t)$ is the displacement vector, and $\mathbf{F}(t)$ is the external force vector including aerodynamic forces and moments.

The structure is discretized into N finite elements, each with n_e nodes, where the displacement within an element is approximated as:

$$\mathbf{u}_e(x,t) = \sum_{i=1}^{n_e} N_i(x)\mathbf{u}_i(t) \tag{2.25}$$

where, $N_i(x)$ is the shape function and $\mathbf{u}_i(t)$ is the nodal displacement. For finite element analysis, classic cubic Hermite shape functions are used to ensure continuity of both displacement and slope.

The element-level mass, stiffness, and damping matrices are given in Eq. 2.20. These matrices are assembled into global matrices for the entire structure.

2.4 Discretization of Structural Domain and Mesh Size Study

The accuracy and reliability of the Finite Element Method (FEM) analyses depend considerably on how the structural domain is discretized, a process known as meshing. Conducting a mesh size study helps ensure accurate results while keeping computational efforts reasonable. This section describes how the structural domain was discretized for the analyses performed in this thesis and outlines the mesh size studies conducted for validation.

In this study, the structural domain, represented by a rectangular wing planform, is divided into finite elements to accurately simulate structural deformations resulting from aerodynamic loads. Four-node quadrilateral (shell) elements are chosen for discretization because they reliably capture bending and torsional behaviors essential for thin structural components. Each of these elements includes four nodes, facilitating precise modeling of the wing's structural responses. The mesh is created systematically across the wing's span and chord, aligning closely with the aerodynamic discretization, thus ensuring accurate fluid-structure interaction.

To confirm that the analysis results are not significantly influenced by mesh density, a mesh independence study was conducted. Starting from a relatively coarse mesh, the mesh was progressively refined. At each refinement step, critical parameters such as tip displacement, maximum stress, and modal frequencies were evaluated until further refinements resulted in minimal change (less than 1%). The mesh densities examined are:

- **Coarse Mesh**: $N_x \times N_y = 8 \times 12$ (96 elements)
- **Intermediate Mesh**: $N_x \times N_y = 16 \times 24$ (384 elements)

- **Fine Mesh**: $N_x \times N_y = 32 \times 48$ (1536 elements)

Rather than adopting a single mesh size universally, mesh size dependency was checked individually for each specific analysis case. Parameters such as tip displacement and modal frequencies were monitored closely for changes across different mesh densities. The final mesh size selected for each analysis ensured negligible variation in critical parameters, confirming solution stability and accuracy without imposing excessive computational demands.

By systematically conducting mesh dependency checks for each analysis scenario, the study ensured accurate modeling of the structural responses relevant to aeroelastic phenomena like flutter and limit cycle oscillations. The approach provided a balance between computational resources and the reliability of results, supporting robust and accurate subsequent coupled aerodynamic-structural analyses.

2.4.1 Boundary Conditions

Accurately defining boundary conditions is essential to ensure the physical realism and accuracy of finite element analyses. For this study, boundary conditions are applied to constrain the structural model, reflecting realistic support conditions found in practical scenarios. Figure 2.8 illustrates the boundary conditions imposed on a thin rectangular plate, highlighting the clamped and free edges.

The specific boundary conditions considered include the following:

- **Clamped (Fixed) Edges:** Edges with clamped boundary conditions are fully restricted, meaning that both translational displacements and rotational movements at these boundaries are zero. This setup simulates scenarios where the edges are rigidly fixed to an immovable support, preventing any motion.

- **Pinned (Simply Supported) Edges:** Pinned edges allow rotational movements while restricting translational displacements to zero. This condition simulates supports such as hinges or simple bearings, permitting rotation but preventing vertical or horizontal translation at the support points.

- **Free Edges:** Edges without imposed constraints, allowing full translational and rotational freedom. The free edges naturally respond to external loads and deform according to the structural and loading conditions, without modifying the global stiffness matrices.
- **Bushing (Spring–Dashpot) Edges:** These edges are connected to a support (or adjacent structure) via generalized bushing elements that provide both stiffness and damping. Translational stiffness coefficients K_{xx}, K_{yy}, K_{zz} and rotational stiffness coefficients K_{rx}, K_{ry}, K_{rz} resist displacements and rotations proportionally, while corresponding damping coefficients $C_{xx}, C_{yy}, C_{zz}, C_{rx}, C_{ry}, C_{rz}$ dissipate energy. Under load, the edge deforms and rotates in a controlled, compliant manner according to the prescribed bushing properties.

Implementing these conditions correctly is crucial, as they directly influence global stiffness and mass matrices, significantly affecting the structural response, eigenvalues, and mode shapes obtained from FEM analyses.

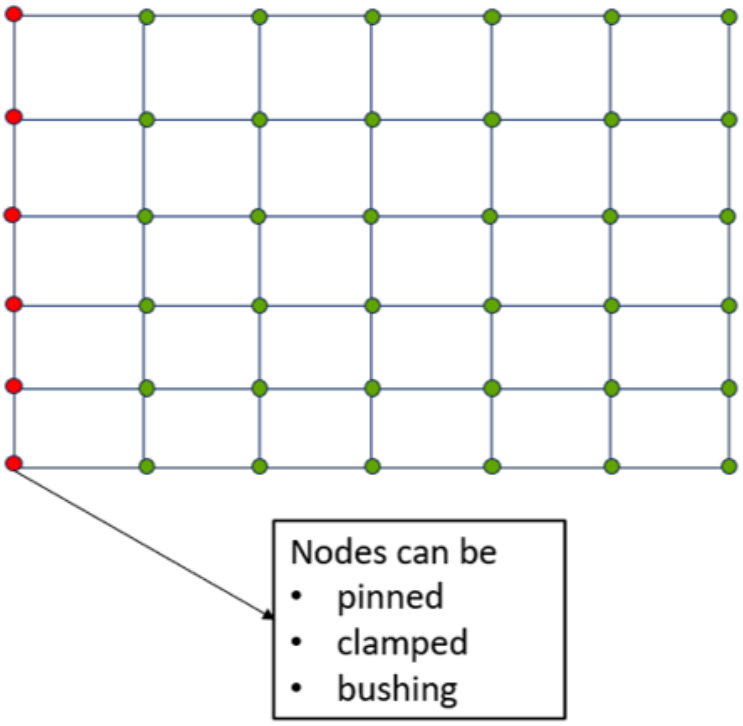

Figure 2.8: Finite element representation of a thin rectangular plate, illustrating clamped and free edges.

2.5 Coupling with Aerodynamics Analysis

To accurately capture the dynamic response of aeroelastic systems such as aircraft wings, structural displacements and rotations calculated using the Finite Element Method (FEM) must be tightly integrated with aerodynamic loads. In this thesis, aerodynamic forces are calculated by the Unsteady Vortex Lattice Method (UVLM), a numerical method effective in modeling unsteady airflow phenomena around flexible structures. The FEM provides the displacements and rotations at every timestep, which are then utilized by the aerodynamic solver (UVLM) to update aerodynamic forces and moments. This creates an iterative loop between the structural and aerodynamic solvers, ensuring the simulation captures the true interactive physics of aeroelastic behavior such as flutter.

To explain this integration clearly, first consider the aeroelastic response using a simplified two-degree-of-freedom (2-DOF) representation (Figure 2.9). An airfoil undergoing vertical translation (plunge, h) and rotational motion (pitch, α) can be described by the following structural dynamic equations:

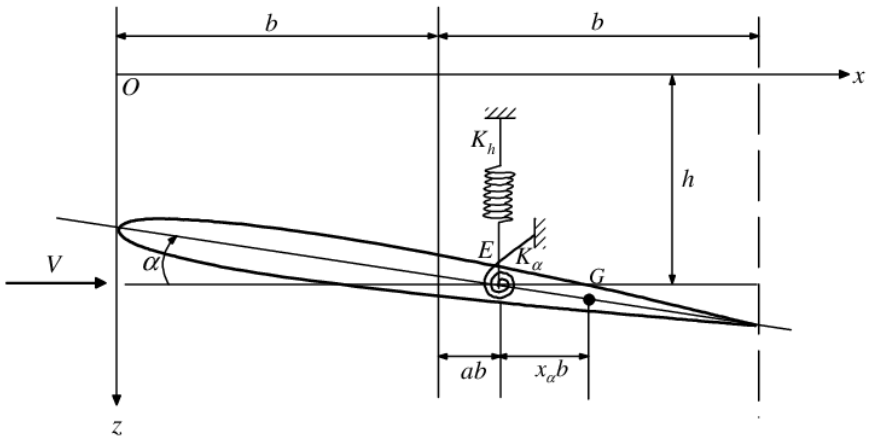

Figure 2.9: Aeroelastic model with 2-DoF system, adapted from [5].

$$m\ddot{h}(t) + S_\alpha \ddot{\alpha}(t) + c_h \dot{h}(t) + k_h h(t) = F_{\text{aero}}(t) \tag{2.26}$$

$$S_\alpha \ddot{h}(t) + I_e \ddot{\alpha}(t) + c_\alpha \dot{\alpha}(t) + k_\alpha \alpha(t) = M_{\text{aero}}(t) \tag{2.27}$$

where,

- m: Mass of the airfoil,
- S_α: Static moment about the elastic axis,
- I_e: Moment of inertia about the elastic axis,
- c_h, c_α: Structural damping coefficients for plunge and pitch,
- k_h, k_α: Structural stiffness coefficients,
- $F_{\text{aero}}(t)$: Aerodynamic lift force,
- $M_{\text{aero}}(t)$: Aerodynamic pitching moment.

The aerodynamic forces $F_{\text{aero}}(t)$ and $M_{\text{aero}}(t)$ are computed using the Unsteady Vortex Lattice Method (UVLM). These forces depend on the airfoil's motion, freestream velocity, and wake-induced effects, leading to a coupled interaction between the structural and aerodynamic domains.

Matrix Form Representation: The above equations are combined into a matrix form:

$$\mathbf{M}\ddot{\mathbf{u}}(t) + \mathbf{C}\dot{\mathbf{u}}(t) + \mathbf{K}\mathbf{u}(t) = \mathbf{F}_{\text{aero}}(t) \tag{2.28}$$

where,

$$\mathbf{M} = \begin{bmatrix} m & S_\alpha \\ S_\alpha & I_e \end{bmatrix}, \quad \mathbf{C} = \begin{bmatrix} c_h & 0 \\ 0 & c_\alpha \end{bmatrix}, \quad \mathbf{K} = \begin{bmatrix} k_h & 0 \\ 0 & k_\alpha \end{bmatrix}, \quad \mathbf{u}(t) = \begin{bmatrix} h(t) \\ \alpha(t) \end{bmatrix}$$

State-Space Formulation: To facilitate numerical simulation, the system is reformulated in a state-space form:

$$\dot{\mathbf{x}}(t) = \mathbf{A}\mathbf{x}(t) + \mathbf{B}\mathbf{f}_{\text{aero}}(t) \tag{2.29}$$

where,

$$\mathbf{x}(t) = \begin{bmatrix} \mathbf{u}(t) \\ \dot{\mathbf{u}}(t) \end{bmatrix}, \quad \mathbf{A} = \begin{bmatrix} \mathbf{0} & \mathbf{I} \\ -\mathbf{M}^{-1}\mathbf{K} & -\mathbf{M}^{-1}\mathbf{C} \end{bmatrix}, \quad \mathbf{B} = \begin{bmatrix} \mathbf{0} \\ \mathbf{M}^{-1} \end{bmatrix}$$

where, $\mathbf{f}_{\text{aero}}(t) = [F_{\text{aero}}(t), M_{\text{aero}}(t)]^T$ represents the aerodynamic forces computed using UVLM.

2.5.1 Coupling Mechanism Between Structure and Aerodynamics

The structural solver provides the current displacement and rotation of the structure at each timestep. These updated structural states are passed to UVLM, which recalculates aerodynamic loads considering the influence of structural motion. These newly computed aerodynamic forces are then fed back into the structural solver, thereby creating an iterative loop. Figure 2.10 illustrates this iterative coupling.

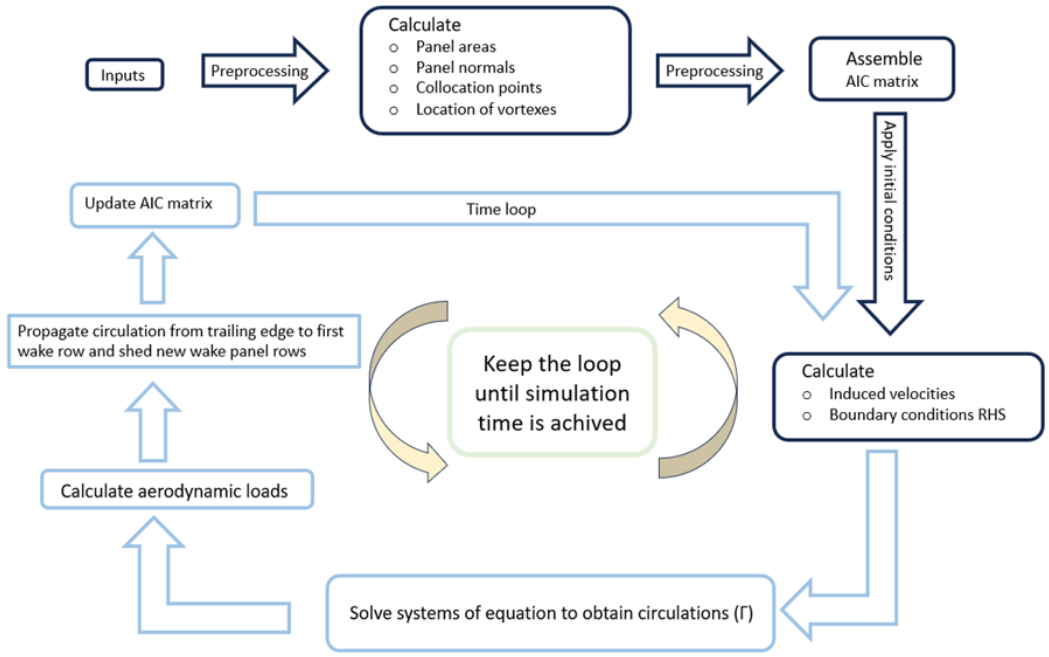

Figure 2.10: Two-way coupling mechanism between structural and aerodynamic solvers.

2.6 Numerical Implementation

The coupled aerodynamic-structural interaction problem is solved iteratively using a time-stepping numerical approach. This methodology ensures accurate representation and synchronization of aerodynamic and structural responses within each discrete time increment. The following steps outline the detailed implementation procedure:

1. **Structural Solver:** At the beginning of each timestep, the structural equations of motion, represented by Eq. 2.28, are solved using a finite-element-based

structural solver. This calculation updates structural parameters such as displacement (h, α) and their corresponding velocities ($\dot{h}$, $\dot{\alpha}$). The solution considers structural mass, damping, stiffness, and external aerodynamic loads from the previous aerodynamic calculations.

2. **Aerodynamic Solver:** The updated structural displacements and velocities are then fed into the aerodynamic solver employing the Unsteady Vortex Lattice Method (UVLM). This solver calculates the aerodynamic forces (F_{aero}) and aerodynamic moments (M_{aero}) by integrating the effect of bound vortices and the wake vortices shed into the flow. Aerodynamic calculations include wake dynamics and vortex-induced velocity fields based on the updated geometry and motion of the structure.

3. **Convergence Check:** Data exchange occurs iteratively between structural and aerodynamic solvers within each timestep until convergence is reached. Convergence is typically evaluated based on the stabilization of displacements, velocities, aerodynamic forces, and moments between successive iterations. This iterative convergence ensures stability and accuracy of the coupled fluid-structure interaction results.

4. **Time Advancement:** Upon achieving convergence, the wake vortices' positions are updated based on their convection velocities, and the simulation progresses to the subsequent timestep. This advancement involves recalculating the wake geometry using both induced velocities from existing vortices and freestream flow contributions.

Wake Dynamics and UVLM Integration: The wake dynamics in UVLM are represented by discrete trailing vortices that evolve downstream based on the local velocity field, governed by the equation:

$$\frac{d\mathbf{r}_{\text{wake}}}{dt} = \mathbf{v}_{\text{ind}} + \mathbf{v}_{\text{freestream}} \tag{2.30}$$

where, $\mathbf{v}_{\text{ind}}$ represents the induced velocity component generated by the bound and trailing vortices, and $\mathbf{v}_{\text{freestream}}$ corresponds to the uniform freestream velocity. This equation is crucial as it accurately predicts the evolution of wake vortex positions,

essential for correctly capturing the wake-induced aerodynamic loading and its influence on structural responses.

2.7 Stability and Flutter Analysis

Flutter is a dynamic instability phenomenon that occurs when aerodynamic forces and structural responses reinforce each other, causing oscillations to transition from stable, damped vibrations to rapidly divergent behaviors. The identification and prediction of flutter conditions involve the following computational approaches:

- **Eigenvalue Analysis:** This approach involves solving the eigenvalue problem formulated by the state-space system equations (see Eq. 2.29). Flutter onset is determined by monitoring eigenvalues of the coupled system as the freestream velocity increases. The critical flutter speed, U_f, is defined as the velocity at which any eigenvalue crosses into the right-half of the complex plane, indicating a transition from stability to instability.

- **Time-Domain Simulations:** Time-domain simulations are performed by numerically integrating the coupled structural and aerodynamic equations over time. These simulations offer detailed insights into the dynamic evolution of aeroelastic behavior, enabling observation of transient behaviors and sustained oscillations characteristic of flutter onset. The simulations are run for varying freestream velocities to identify the conditions under which sustained oscillations, characteristic of flutter or limit cycle oscillations (LCOs), emerge.

Validation Cases: To ensure the robustness and accuracy of the developed coupled analysis tool, several well-documented validation cases are employed. These include:

1. **Two-Dimensional Validation:** The analysis tool is first validated against analytical solutions, such as those provided by Theodorsen's aerodynamic theory, for simple two-dimensional airfoil configurations undergoing prescribed pitch and plunge motions.

2. **Three-Dimensional Validation:** The tool is further validated by comparing simulation results with experimental wind tunnel data available in the literature for the three-dimensional wing configurations. Such experimental comparisons are essential to demonstrate the accuracy of the model in predicting realistic flutter speeds for more complex aerodynamic and structural interactions.

2.8 Summary

In this chapter, the integrated computational methodology developed for aeroelastic analysis has been thoroughly detailed. The aerodynamic model based on the Unsteady Vortex Lattice Method (UVLM) accurately predicts unsteady aerodynamic loads by incorporating vortex shedding and wake dynamics. Structural responses are modeled using Finite Element Method (FEM), enabling precise simulation of dynamic deformation, plunge, and pitch behaviors. The iterative coupling between aerodynamic and structural solvers ensures realistic interactions essential for analyzing complex phenomena like flutter and limit cycle oscillations. This robust computational framework, validated through well-documented analytical and experimental test cases, provides the foundation for the validation studies and aeroelastic simulations presented in Chapter 3.

CHAPTER 3

VALIDATION SIMULATIONS AND RESULTS

In this Chapter, several validation test cases are presented to demonstrate the capabilities of the in-house computational aeroelastic analysis tool developed in this thesis. A chordline representation of an airfoil with dynamic motion (2-D validation cases) and a planar surface representation of a wing (3-D validation cases) are employed to confirm the accuracy of both the aerodynamic and structural solvers, as well as the coupled aeroelastic framework. The purpose of this Chapter is to show that the coupled UVLM/FEM aeroelastic analysis tool can reproduce known aeroelastic responses. Specifically, the predictions by using the analysis tool are compared against two well-established experimental test cases, both involving two-degree-of-freedom (2-DOF) flat plate configurations in low-speed wind tunnel tests.

To assess the accuracy of the in-house codes for steady-state and unsteady aeroelastic analyses, the following validation test cases are studied:

- **Aerodynamic validation only:**
  - 2-D UVLM simulations with free wake (static and dynamic prescribed motions).
  - 3-D wing simulations with free wake (steady aerodynamic loads).
- **Structural validation only:**
  - 3-D wing structural deformations under given steady-state aerodynamic loads.
- **Coupled Aeroelastic validation:**
  - 2-DOF flat plate flutter test based on Amandolese et al. [41].

The key objectives of the validation studies are summarized as follows:

- To verify the aerodynamic analysis part by using only the Vortex Lattice Method (VLM) with free-wake modeling for 2-D and 3-D test cases.
- To validate the structural analysis part using the FEM solver under static aerodynamic loads for selected cases.
- To ensure that the UVLM/FEM coupled analysis tool can predict the flutter onset speed in agreement with the experimental data.
- To check the robustness of the predictions as numerical parameters (e.g., mesh density, time-step size) are refined.

3.1 2-D/3-D Validation Studies for Aerodynamic Analysis

The aerodynamic validation focuses on assessing the accuracy of the in-house Vortex Lattice Method (VLM) with wake roll-up capabilities for both two-dimensional (2-D) and three-dimensional (3-D) test cases. These test cases are designed to confirm that the solver can capture steady-state and unsteady flow characteristics, including the distribution of aerodynamic loads, the behavior of freely convecting wakes, and the correct partition of circulatory and non-circulatory (added-mass) contributions in unsteady lift. The validation test cases for aerodynamic analyses encompasses two main configurations:

- 2-D Airfoil Test Cases (Static and Dynamic Motion)
- 3-D Wing Test Case (Steady Loads)

3.1.1 2-D Airfoil (Flat Plate): Steady-State Test Case

An airfoil at a given angle of attack is selected as a steady-state test case and the results are compared with the data available from literature.

A first step in verifying the aerodynamic solver is to compare the computed aerodynamic coefficients for a two-dimensional airfoil at a fixed angle of attack (AoA) with known reference data. For this purpose:

- A chordline representation of the flat plate is modeled using a panel-based VLM approach in which the chord is divided into panels for discretizing the bound vortex.
- A *free wake* condition is imposed, allowing the wake vortices to shed from the trailing edge and convect downstream at the local flow velocity.
- The circulation distribution along the airfoil and the resulting lift and moment coefficients are computed.

Validation in the static AoA regime typically involves comparisons to:

- Analytical solutions (e.g., potential flow or thin airfoil theory) when the angle of attack is relatively small.
- Published results from other computational methods, such as panel codes or vortex methods, which capture the essential 2-D inviscid flow physics.

In general, the in-house code is expected to reproduce the linear lift curve slope near small AoA accurately. At higher angles of attack, the inviscid nature of the VLM can introduce some discrepancies due to flow separation not being modeled. Nevertheless, for moderate angles, the match with known reference solutions is typically strong, indicating that the solver correctly implements the potential flow formulation and boundary conditions.

3.1.2 2-D Airfoil (Flat Plate): Unsteady Test Case

Dynamic motion of a pitching and plunging airfoil is selected as an unsteady validation test case and the results are compared with analytical solution of Theodorsen's Function.

A more stringent test of the aerodynamic solver is to simulate a two-dimensional airfoil undergoing prescribed pitching or plunging motions. In these unsteady cases:

- The airfoil is given a known time-dependent rotation (pitch) around a pivot point or a specified vertical displacement (plunge).
- The wake geometry is updated at each time step to reflect the new trailing edge position and the convective transport of shed vortices.
- The unsteady aerodynamic forces and moments are extracted over time for comparison with either analytical (e.g., Theodorsen's theory) or existing numerical/experimental data.

Because unsteady aerodynamic loads depend on vortex shedding and wake interactions, validating the free-wake approach is critical. Good agreement with Theodorsen's lift and moment predictions over a range of reduced frequencies suggests that the solver correctly models both **circulatory** effects (due to bound circulation and trailing-edge vortex shedding) and **non-circulatory** effects (the added-mass or inertial contributions).

Circulatory vs. Non-Circulatory Lift Contributions: In unsteady motion, the total lift $C_{L,\text{total}}$ can be decomposed into:

$$C_{L,\text{total}} = C_{L,\text{circ}} + C_{L,\text{nc}} \tag{3.1}$$

where $C_{L,\text{circ}}$ arises from the circulation bound to the airfoil (and its interaction with the wake), and $C_{L,\text{nc}}$ is the non-circulatory or added-mass term arising from accelerating the surrounding fluid.

Theodorsen's Function: Theodorsen's classical solution expresses the unsteady lift on a thin airfoil in harmonic motion through a frequency-dependent function $C(k)$, known as *Theodorsen's Function*, where $k = \omega c/2U_\infty$ is the reduced frequency:

$$C(k) = \frac{H_1^{(2)}(k)}{H_1^{(2)}(k) + i\, H_1^{(1)}(k)} \tag{3.2}$$

and $H_1^{(1)}$, $H_1^{(2)}$ are the first-order Hankel functions of the first and second kind, respectively. This function quantifies how circulatory effects lag behind the harmonic motion of the airfoil, thereby modifying the phase and amplitude of the unsteady aerodynamic forces.

3.1.2.1 Results and Discussions

From the simulation results and comparisons with the theory for pitching/plunging sinusoidal motion, Figures 3.1 3.2 3.3 3.4 3.5 3.6 illustrate a representative comparison of lift coefficients when wakes are turned off from UVLM code defined as below:

1. **Steady Lift**: The baseline C_L for the same static angle of attack.

2. **Theodorsen's Prediction**: Analytical solution for a pitching or plunging airfoil in sinusoidal motion.

3. **Circulatory Contribution**: The portion of the computed lift from bound circulation and shed vortices.

4. **Non-Circulatory Contribution**: The added-mass term reflecting the inertia of the fluid.

5. **Total Lift (Circulatory + Non-Circulatory)**: The sum of the circulatory and non-circulatory components, which should match the Theodorsen reference closely if the solver is accurate.

Good agreement with Theodorsen's function indicates accurate modeling of unsteady circulatory and added-mass effects.

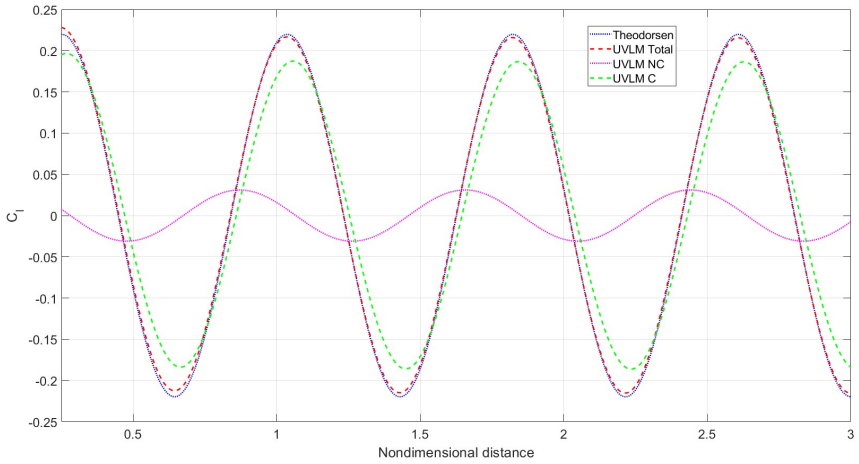

Figure 3.1: Comparison of lift coefficients for a pitching airfoil (k = 0.25): Theodorsen's (analytical), Circulatory UVLM ($C_{L,\text{circ}}$), Non-Circulatory UVLM ($C_{L,\text{nc}}$), Total UVLM.

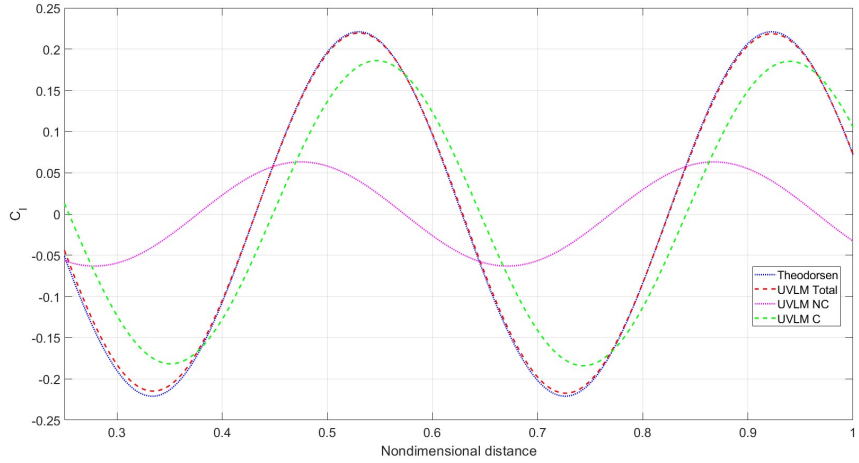

Figure 3.2: Comparison of lift coefficients for a pitching airfoil (k = 0.5): Theodorsen's (analytical), Circulatory UVLM ($C_{L,\text{circ}}$), Non-Circulatory UVLM ($C_{L,\text{nc}}$), Total UVLM.

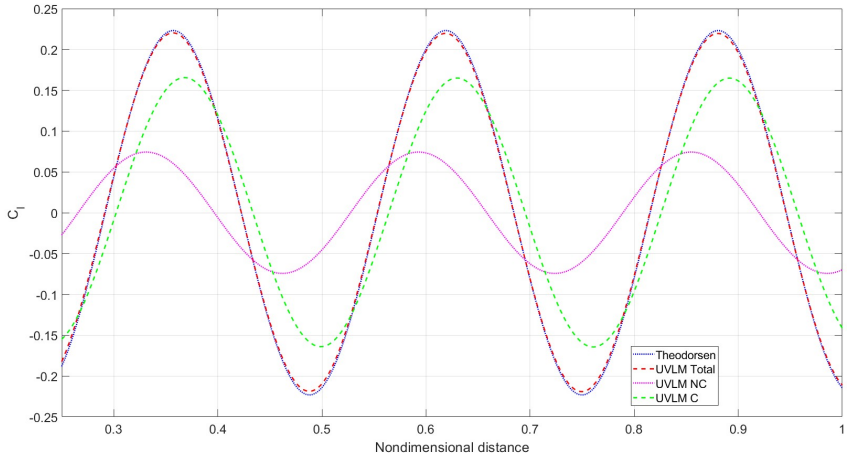

Figure 3.3: Comparison of lift coefficients for a pitching airfoil (k = 0.75): Theodorsen's (analytical), Circulatory UVLM ($C_{L,\text{circ}}$), Non-Circulatory UVLM ($C_{L,\text{nc}}$), Total UVLM.

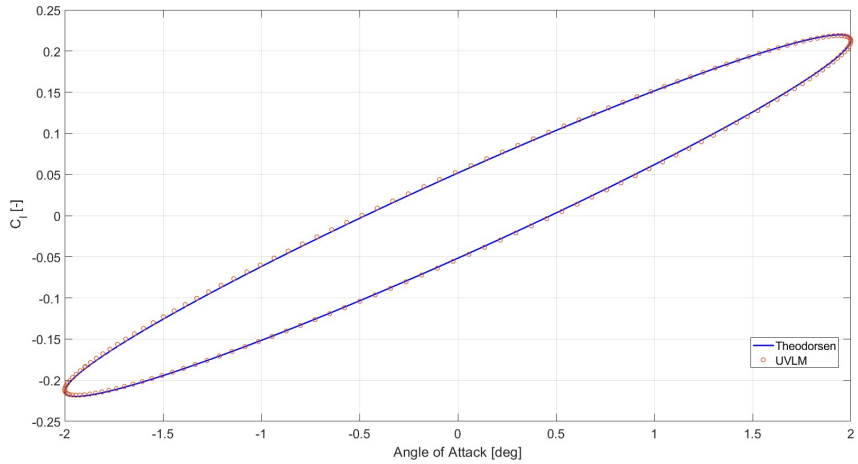

Figure 3.4: Lift coefficient for pitching airfoil for k=0.25

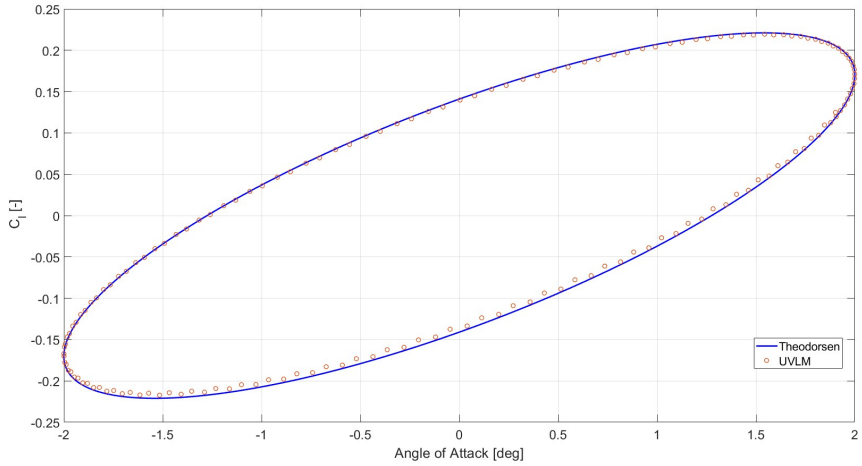

Figure 3.5: Lift coefficient for pitching airfoil for k=0.5

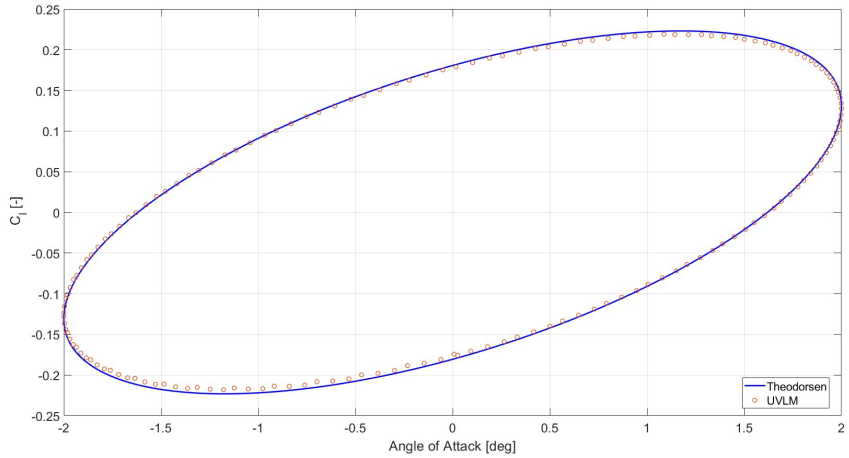

Figure 3.6: Lift coefficient for pitching airfoil for k=0.75

The key findings for 2-D unsteady calidation test case can be summarized as:

- **Agreement with Theodorsen's Theory:** The computed total lift matches the amplitude and phase predicted by Theodorsen's function for small-to-moderate reduced frequencies.

- **Circulatory and Non-Circulatory Decomposition:** Separate tracking of $C_{L,\text{circ}}$ and $C_{L,\text{nc}}$ shows physical consistency with added-mass and wake shedding phenomena.

- **Sensitivity to Reduced Frequency:** At higher k values, discrepancies can emerge from the simplified inviscid assumptions, yet the solver still captures the major trends.

Figures 3.7 3.8 3.9 3.10 schematically illustrate the chordline model and the free wake behind it for a pitching airfoil, highlighting how vortex elements are continuously generated at the trailing edge and convected downstream, influencing the circulatory component of the unsteady lift.

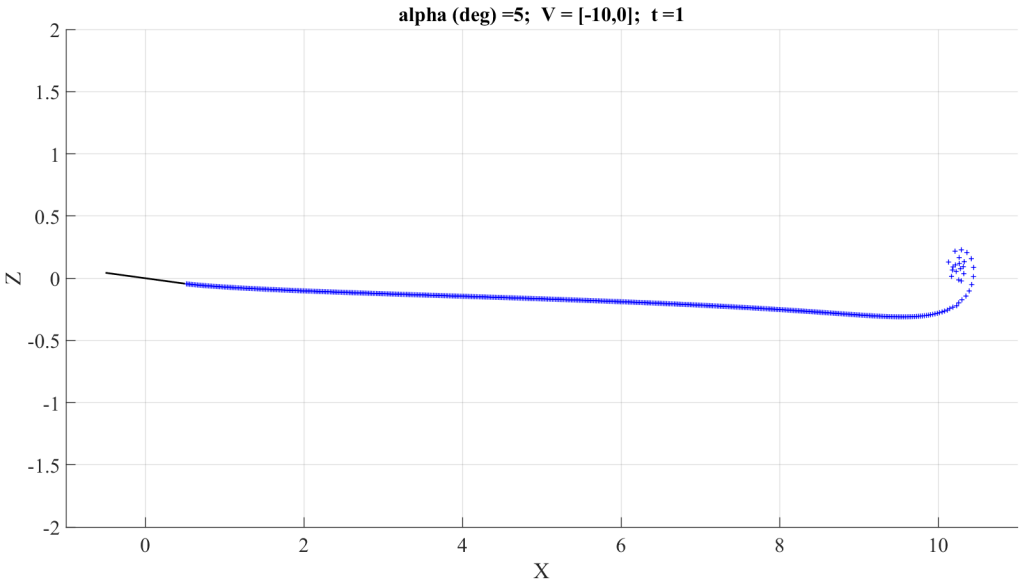

Figure 3.7: Wake formation for reduced frequency is zero (no oscillation) and time step is 0.002.

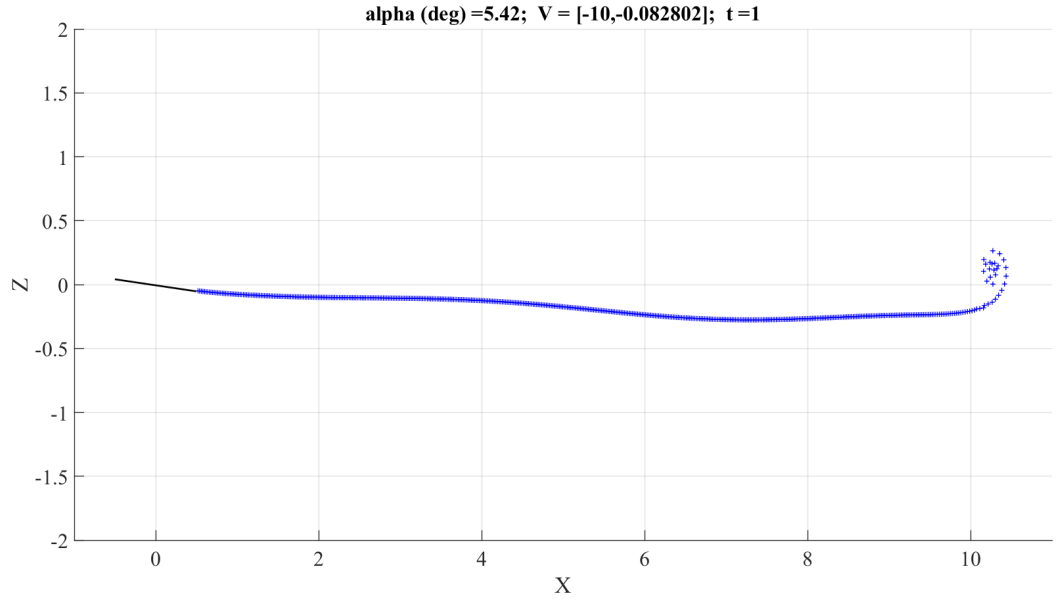

Figure 3.8: Wake formation for reduced frequency is 0.1 and time step is 0.002 with small amplitude.

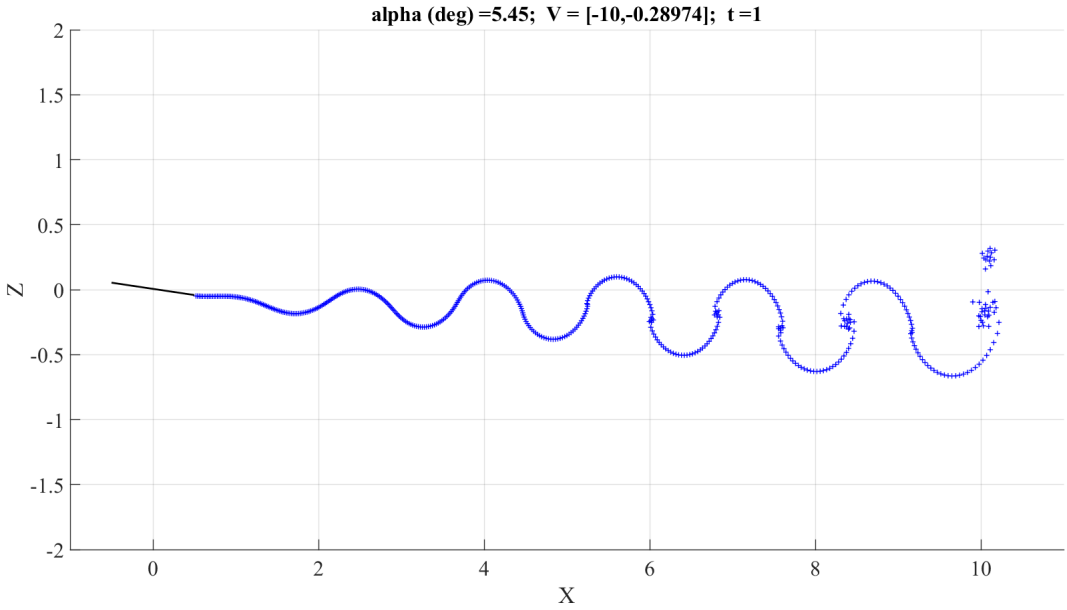

Figure 3.9: Wake formation for reduced frequency is 0.4 and time step is 0.002 with small amplitude.

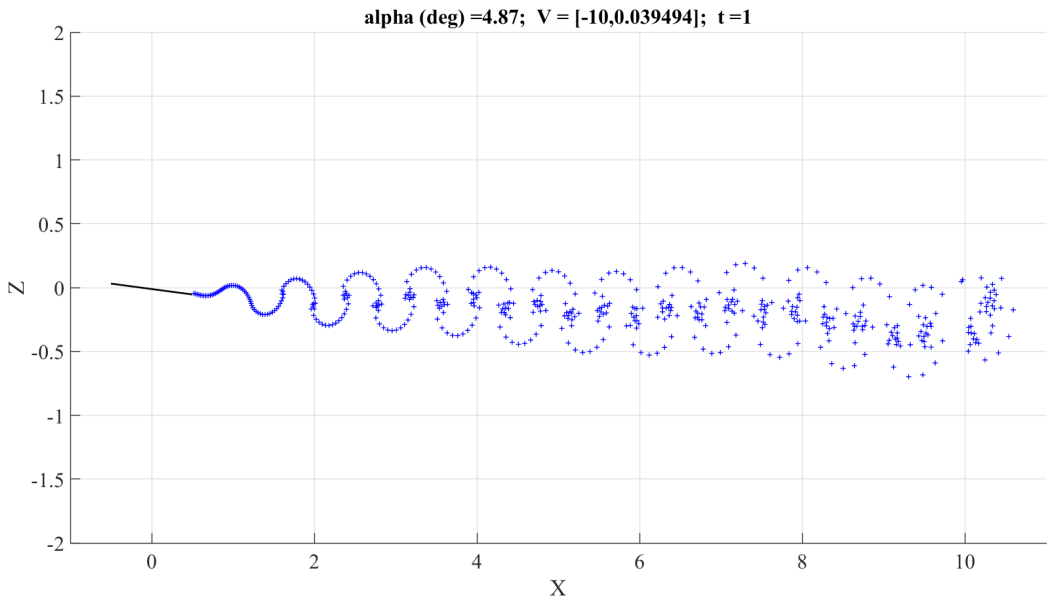

Figure 3.10: Wake formation for reduced frequency is 0.8 and time step is 0.002 with small amplitude.

3.1.3 3-D Wing: Steady-State Test Case

In addition to the two-dimensional verification, the aerodynamic code is tested for a three-dimensional finite wing under a constant freestream velocity and steady angle of attack. Unlike the 2-D airfoil, the 3-D wing experiences spanwise flow variations, tip vortices, and other distinctly three-dimensional effects. For validation case, a rectangular plate is divided into a network of surface panels in the streamwise and spanwise directions. The trailing edge panels continuously shed vortex filaments into the wake, which are then convected downstream in a free-wake manner, capturing tip vortex roll-up.

3.1.3.1 Lift Calculations

The theoretical lift coefficient can be calculated by Prandtl's Lifting-Line (LL) Theory approximation for a finite wing (at low α) with a thin airfoil (0.5% thickness-to-chord

ratio) by using the following relations for lift coefficient change with alpha given as:

$$\frac{dC_L}{d\alpha} = \frac{2\pi\, AR}{AR + 2} \tag{3.3}$$

where, $AR = b^2/S$ is aspect ratio, b is span, $S = (b)(c)$ is planform area, c is chord, and α is angle of attack, and lift coefficient and lift given as:

$$C_L = \left(\frac{dC_L}{d\alpha}\right)\alpha \tag{3.4}$$

$$L = \frac{1}{2}\,\rho\, V^2\, S\, C_L \tag{3.5}$$

where, V is freestream velocity and ρ is air density.

The numerical lift calculation is obtained from the steady-state Vortex Lattice Method (VLM) simulation with selected sample geometric and flow parameters of $AR = 6.42857, \rho = 1.225\,\text{kg/m}^3, V = 10\,\text{m/s}$, and $\alpha = 5^\circ$ and compared with the Prandtl's LL theory lift calculation as $L_{VLM} = 11.02$ N and $L_{LL} = 11.21$ N. Comparing with the theoretical prediction, the difference is about 1.7%. This reasonable agreement validates both the analytical approach and the VLM numerical results for the given conditions.

The aerodynamic validation efforts, encompassing both 2-D and 3-D test cases, and steady and unsteady conditions, demonstrate that the in-house solver is capable of capturing essential inviscid aerodynamic behavior. Specifically:

- **2-D Agreement with Theodorsen's Theory:** Good alignment with Theodorsen's function for pitching/plunging motions confirms the proper modeling of circulatory and non-circulatory (added-mass) effects in unsteady flows.
- **3-D Agreement:** Consistent predictions of spanwise loading and induced drag suggest the solver can handle finite-wing effects accurately.
- **Robust Free-Wake Implementation:** The free-wake roll-up methodology provides realistic wake shapes and downstream vortex structures without manual wake modeling, a key feature for aeroelastic simulations where the wake must adapt to moving structures.

Overall, these validated aerodynamic capabilities lay the groundwork for coupling with the structural solver to perform fully fledged aeroelastic simulations, as discussed next.

3.2 Validation Studies for Structural Analysis: Steady-State Test Case

In this section, a validation test case is presented for the structural analysis. Both an analytical method and Finite-Element (FE) analyses in ABAQUS CAE, and an in-house Finite-Element Method (FEM) code are presented for a rectangular steel plate of a given span. The main objective is to compare the tip deflection predicted by simple beam theory with those obtained from the numerical models.

A steel plate with $6.428\,\mathrm{m}$ span, $1.0\,\mathrm{m}$ chord, and $10\,\mathrm{mm}$ thickness, subjected to a lift force of $23.25\,\mathrm{N}$ at 1° angle of attack is selected as a test case.

3.2.1 Analytical Beam Theory Approach

The analytical beam theory calculations are performed for the selected test case of the beam structure by assuming uniformly distributed total lift force and by using the following parameters:

- **Material:** Steel with Young's modulus $E = 2.0 \times 10^{11}\,\mathrm{Pa}$ and Poisson's ratio $\nu \approx 0.3$.
- **Geometry:** Span of $b = 6.428\,\mathrm{m}$, chord of $c = 1.0\,\mathrm{m}$, and thickness of $t = 10\,\mathrm{mm} = 0.01\,\mathrm{m}$.
- **Total Lift Force:** $L = 23.25\,\mathrm{N}$ (assumed uniformly distributed for the beam-theory approximation).
- **Second Moment of Area (Flat Plate):**

$$I = \frac{c\,t^3}{12} = \frac{(1.0)\,(0.01)^3}{12} = 8.33 \times 10^{-8}\ \mathrm{m}^4 \tag{3.6}$$

- **Boundary Condition:** A cantilever assumption (one long edge fully fixed, the other free).

The total lift force L is modeled as a uniform load w over the span:

$$w = \frac{L}{b} \tag{3.7}$$

For a cantilever beam of length b with uniform load w, the maximum deflection at the free end is given by:

$$\delta_{\max} = \frac{w\, b^4}{8\, E\, I} \tag{3.8}$$

The calculations yield as $\delta_{\max} \approx 0.045$ m $= 45$ mm. This estimate assumes linear elasticity and small deflections.

3.2.2 Finite-Element Analyses: ABAQUS CAE Model

The same beam is modelled by using ABAQUS CAE with the same parameters and following properties:

- **Elements:** Shell elements are used
- **Boundary Conditions:** One long edge (root) fully clamped. The opposite edge is free.
- **Load Application:** A pressure distribution obtained from a VLM (Vortex Lattice Method) code is applied to the surface in ABAQUS CAE.

The integrated total force for this case corresponds to $23.25\,\mathrm{N}$.

3.2.3 Finite-Element Analyses: In-house FEM Code Model

An independent in-house FEM code is developed and used with the same parameters, boundary conditions, and material properties. The identical pressure field was imposed, ensuring the same total force of $23.25\,\mathrm{N}$. The results are compared in the next section.

3.2.4 Results and Discussions

Figures 3.11 and 3.12 show the deflection contours from ABAQUS and the in-house FEM code, respectively. Both results are very close, with a tip deflection of approximately $45\,\mathrm{mm}$ to $46\,\mathrm{mm}$. This good agreement confirms the consistency of the linear structural model and the appropriateness of applying the lift as a distributed pressure in order to capture realistic stress and deflection distributions.

It is often questioned whether the total lift should be applied as a single force at the aerodynamic center or distributed as a pressure. In structural analyses, distributing the force (pressure) across the lifting surface typically yields more accurate stress and deflection distributions. A single concentrated load can replicate the net force and moment, but will not capture local stress variations or deformation gradients. Therefore, for this validation, the lift force was distributed according to the VLM pressure field, as shown in the FE simulations.

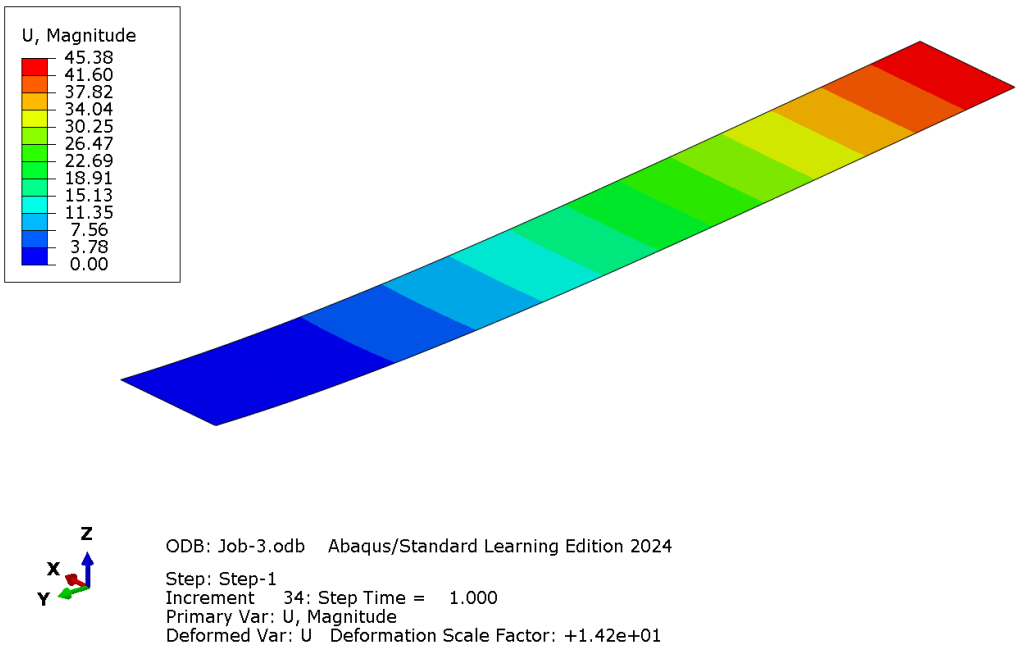

Figure 3.11: ABAQUS CAE deflection contour showing a maximum tip displacement of about $45\,\mathrm{mm}$.

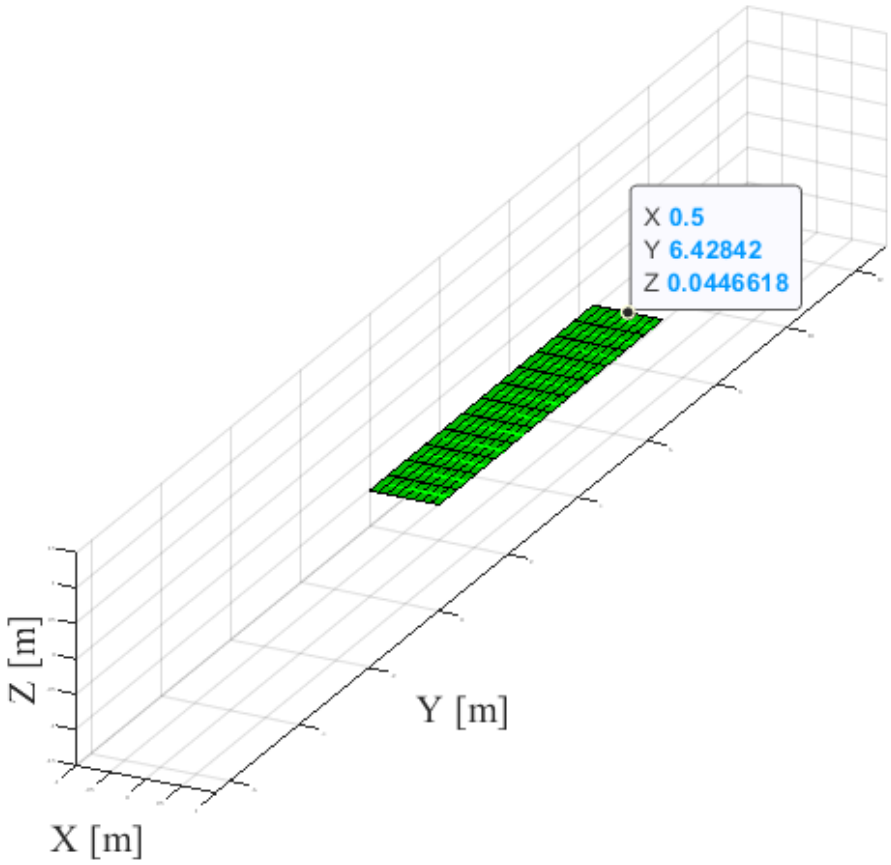

Figure 3.12: Independent FEM code deflection result, with a maximum tip displacement near $44.66\,\mathrm{mm}$.

3.3 Validation Studies for Aeroelastic Analysis: Unsteady Test Case

To establish the foundations of the coupled UVLM/FEM framework, a baseline aeroelastic benchmark is used, a 2-DOF flat plate test case. This involves a flat plate constrained to pitch and plunge degrees of freedom. The experiments for this configuration typically provide:

- Flutter onset speed and the corresponding natural frequency at onset.
- A clear transition from stable motion (below flutter speed) to divergent or self-sustained oscillations (above flutter speed).

Because this system is relatively simple, it serves as an ideal starting point to confirm

the aeroelastic stability predictions of the coupled UVLM/FEM tool. Beyond the linear flutter regime, nonlinear effects often become significant, leading to limit cycle oscillations (LCOs). Amandolese et al. [41] conducted detailed experiments on a 2-DOF flat plate in a wind tunnel, documenting:

- The critical flutter onset speed under low-speed conditions.
- The amplitude and frequency of the limit cycle oscillations once the system is driven into the nonlinear regime.

By reproducing these conditions numerically, the in-house tool's ability to predict both the initial flutter speed, amplitude and frequency can be assessed. Any discrepancies offer insights into possible modeling limitations such as the absence of viscous effects in the UVLM or simplifications in the structural representation.

Computational Simulations and Parameters: The simulation parameters for pitch and plunge motions chosen for the validation case are listed in Table 3.1. These values match the experimental setup by Amandolese et al. [41] as closely as possible.

Table 3.1: Simulation parameters

$M\,[kg]$	$I_\alpha\,[kgm^2]$	$C_h\,[Ns/m]$	$C_\alpha\,[Nms/rad]$	$K_h\,[N/m]$
0.304	4.66×10^{-5}	5.38×10^{-2}	7.91×10^{-5}	595.6

$K_\alpha\,[Nm/rad]$	$\omega_h\,[Hz]$	$\omega_\alpha\,[Hz]$	$S_\alpha\,[m]$	$X_{\text{CG}}\,[m]$
0.149	44.26	56.55	8.48×10^{-4}	2.8×10^{-3}

The geometry and material properties and the flow conditions for this test case can be summarized as:

- **Geometry and Material Properties:** The flat plate dimensions, inertia values, and stiffness coefficients mirror the experimental setup.
- **Flow Conditions:** The freestream velocity is incrementally varied around the flutter onset range. The UVLM assumes incompressible and inviscid flow,

which is appropriate for the low-speed conditions of the experiment.

Numerical Methodology: At each time step, the in-house aerodynamic solver (UVLM) and the in-house structural solver (FEM), the coupled UVLM/FEM solver, AeroWing, exchange information as:

1. The structural solver provides the instantaneous pitch and plunge displacements.

2. The aerodynamic solver updates the wake geometry, circulation distribution, and aerodynamic forces based on these displacements.

3. The updated forces are fed back to the structural solver to obtain the new displacement for the next time step.

4. This coupling continues until convergence at every time increment.

3.3.1 Results for Flutter Analysis

Figures 3.13 and 3.14 show the time history of plunging and pitching motions, respectively. In the experiments by Amandolese et al. [41], the critical flutter speed was reported to be around $U_c = 10.2\,\text{m/s}$. Numerically, the in-house tool predicts a similar critical flutter speed of $U_c \approx 10.7\,\text{m/s}$, reflecting a promising correlation with the reference data.

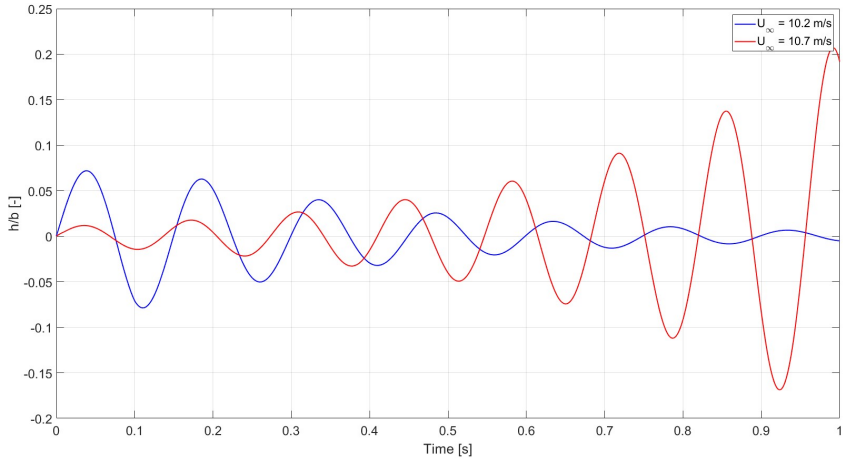

Figure 3.13: Time history of plunging motion

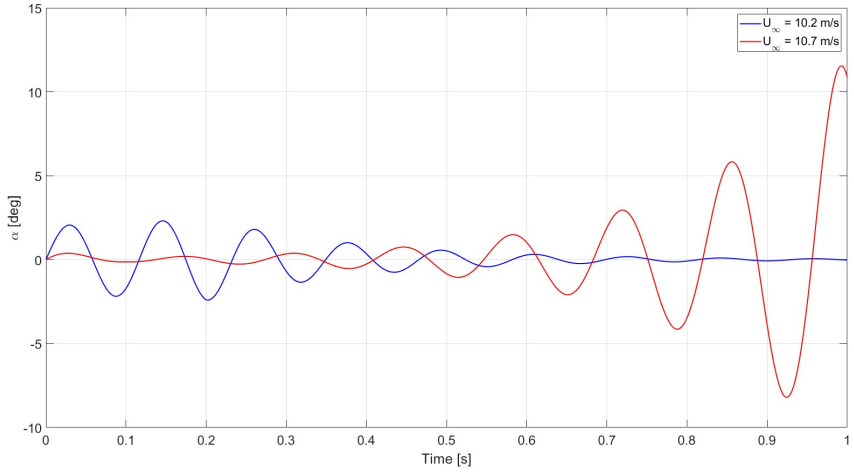

Figure 3.14: Time history of pitching motion

The free wake shape is shown for the subcritical (Figure 3.15) and supercritical cases (Figure 3.16), highlighting the distinct wake patterns before and after flutter onset. As the flow speed increases past U_c, the wake vorticity and aerodynamic coupling sustain the structural oscillations.

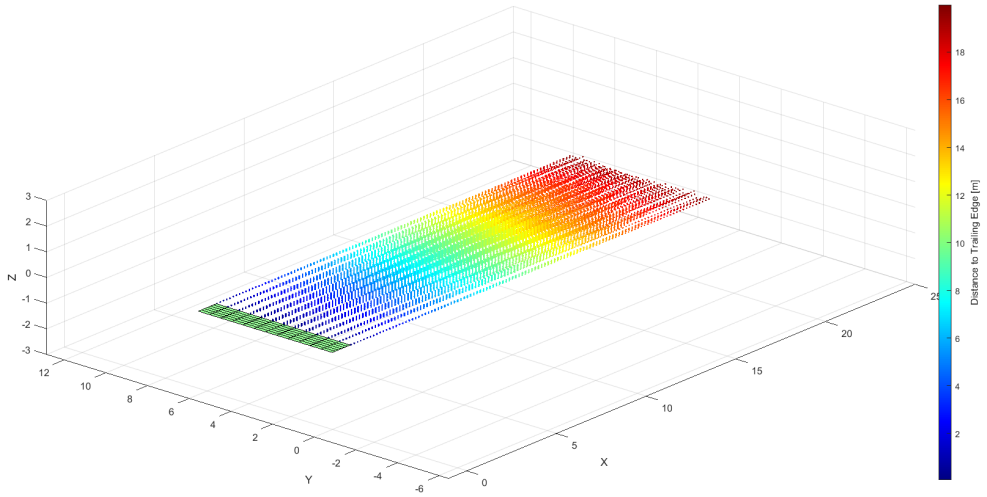

Figure 3.15: Free wake demonstration after the flutter speed.

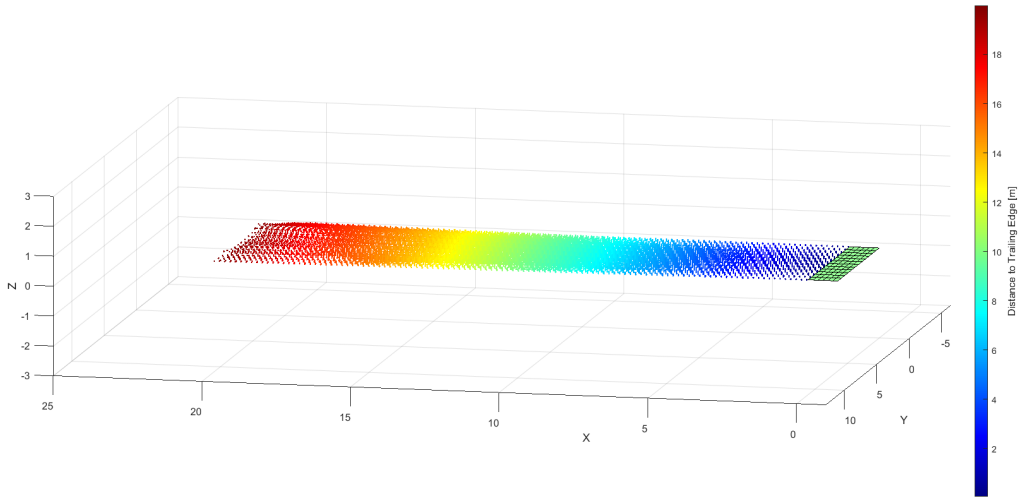

Figure 3.16: Free wake demonstration after the flutter speed.

3.4 Summary and Discussions

The validation efforts have provided us with a great deal of confidence in the computational framework.

- **Reliable Performance of the UVLM/FEM Framework:** The coupled model

effectively predicts the flutter onset speed of a 2-DOF flat plate, matching closely with experimental results reported by Amandolese et al. [41].

- **Robustness in the Nonlinear Regime:** The coupled model can capture the unsteady interactions between aerodynamics and structural response.
- **Minor Sensitivities to Modeling Assumptions:** As with any model, slight discrepancies can arise from uncertainties in material properties, the level of mesh refinement, or the simplified nature of the inviscid flow assumptions in the UVLM. However, these differences are small and do not significantly affect the overall trends or the predictive accuracy of the model.

CHAPTER 4

AEROELASTIC APPLICATIONS AND RESULTS

The primary motivation behind this chapter is to demonstrate the applicability and effectiveness of the developed computational aeroelastic framework by conducting comprehensive numerical analyses on practical aeroelastic scenarios. Aeroelastic phenomena, especially flutter, pose critical challenges to the structural integrity and operational safety of modern aircraft. With the contemporary trend towards increasingly lightweight and flexible aerospace structures, driven by demands for higher efficiency, performance, and mission capability, understanding and accurately predicting aeroelastic behavior becomes paramount. Flutter, a self-excited aeroelastic instability, arises from the dynamic interaction between aerodynamic forces, structural elasticity, and inertial effects. It can rapidly escalate from small initial perturbations into catastrophic structural oscillations, leading to potential structural failures and compromising flight safety. The accurate prediction and management of flutter are therefore vital during the initial design stages of aerospace vehicles. The applications presented in this chapter specifically investigate critical aeroelastic scenarios such as external mass attachments on aircraft structures and fully clamped wing configurations, both of which are frequently encountered in aerospace engineering practice. External payloads—including missiles, fuel tanks, sensors, and other equipment—significantly influence aeroelastic stability by altering the mass distribution, inertia characteristics, and aerodynamic interactions of aircraft wings. Understanding the effects of these attachments is crucial to maintaining structural integrity and ensuring flight safety in both military and commercial aviation contexts. Similarly, fully clamped wing configurations provide a fundamental scenario for validating aeroelastic analysis tools. Investigating such configurations helps establish baseline aeroelastic stability characteristics, which are essential for validating computational methodologies and guiding

structural design choices. By systematically addressing these practical scenarios, this chapter aims not only to validate the computational aeroelastic analysis tool developed in this thesis but also to provide valuable insights and practical recommendations for aerospace engineers. The outcomes of these investigations contribute directly to enhancing aircraft reliability, performance optimization, and safety, aligning with contemporary aerospace industry demands and regulatory requirements.

4.1 Flutter Analysis of a Clamped-Wing Configuration

This section presents a detailed computational investigation of aeroelastic behavior for a clamped-wing configuration, specifically a wing clamped at the root and free at the tip. This scenario is fundamental for validating computational aeroelastic tools, providing essential baseline data on structural stability and flutter characteristics. Such a boundary condition closely resembles practical aerospace applications, including fixed-wing aircraft wings and rotor blades, where structural constraints are applied at one end while the opposite end remains free.

Investigating aeroelastic responses of a wing clamped at the root is particularly beneficial because it isolates the fundamental aerodynamic-structural interactions, simplifying the boundary conditions and allowing clearer interpretation of results. This setup serves as an effective benchmark for validating numerical methodologies against established experimental data and analytical solutions.

The wing considered in this study is modeled as a uniform rectangular aluminum plate. The structural parameters and material properties employed in the simulations are summarized in Table 4.1.

Modal analysis is conducted to determine the fundamental vibrational characteristics of the clamped-wing model. The first three mode shapes, first bending, first torsion, and second bending, are presented in Figure 4.1, along with their corresponding natural frequencies.

The critical flutter speed and corresponding frequency identified from these computational analyses flutter speed is 9.8 m/s and flutter frequency is 8.3 Hz.

Table 4.1: Plate material and geometric parameters

Property	Value
Chord length	152.4 mm
Span	114.3 mm
Thickness	1.727 mm
Young's modulus	18.4 MPa
Density	1230 kg/m^3

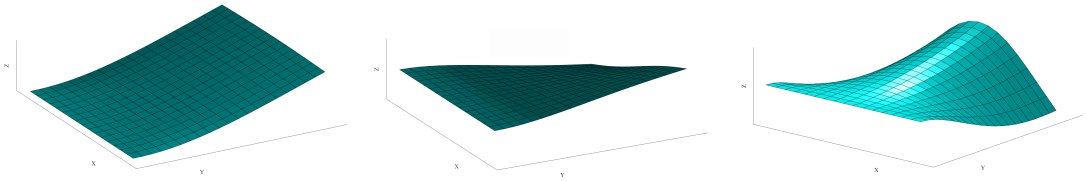

(a) First bending, 1.6075 Hz (b) First torsion, 4.4532 Hz (c) Second bending, 9.7500 Hz

Figure 4.1: First three mode shapes of the clamped-wing configuration.

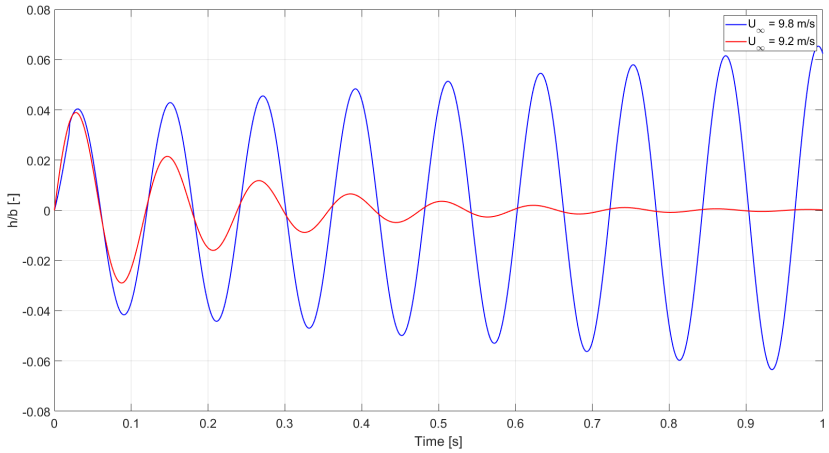

Figure 4.2: Time history of tip displacement

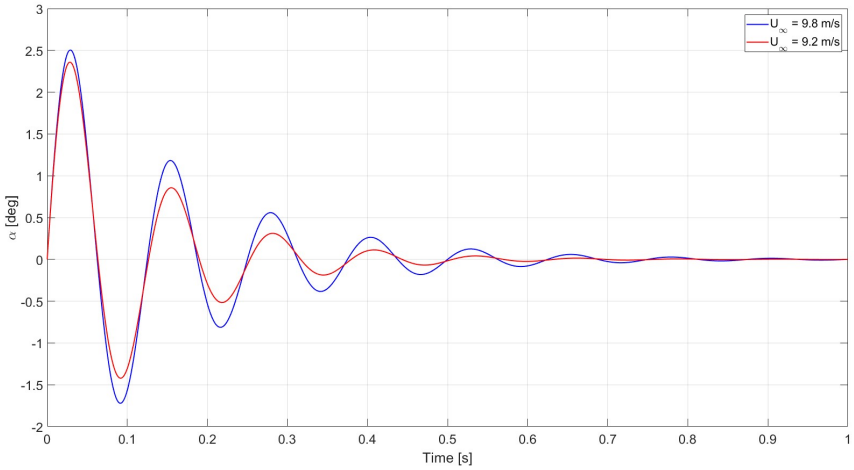

Figure 4.3: Time history of twist angle

This analysis clearly illustrates that the clamped-wing configuration exhibits distinct flutter characteristics, driven primarily by bending-torsion coupling effects shown in Figure 4.2 and Figure 4.3. The determined flutter speed serves as a crucial validation point for the computational aeroelastic solver and provides foundational data for future investigations involving more complex structural constraints and aerodynamic interactions.

4.2 External Mass Attachment Study

Lightweight aircraft structures frequently carry external stores—fuel tanks, missiles, or sensors—that can markedly alter mass and inertia distributions. Such attachments modulate flutter behavior by introducing localized inertia effects and shifting modal interactions. This study quantifies how spanwise store placement affects flutter margins, thereby validating the coupled UVLM–FEM solver and informing guidelines for safe payload integration [42]. A uniform aluminum plate (wing) of span $L = 1.2192\,\mathrm{m}$ and semi-chord $b = 0.1016\,\mathrm{m}$ is modelled. The plate is clamped at the root and free at the tip. A rigid store of mass $M_s = 1.578\,\mathrm{kg}$ (rotational inertia $I_s = 0.0185\,\mathrm{kg{\cdot}m^2}$) is attached at four spanwise locations X_s measured from the root. Material and aerodynamic parameters are listed in Table 4.2. The first three structural modes are retained: the fundamental bending, first torsion, and second bending re-

duced model, which captures over 95% of the dynamic energy in the relevant speed range.

Table 4.2: Physical properties of the plate and store

Parameter	Symbol	Value
Plate span	L	1.2192 m
Semi-chord	b	0.1016 m
Plate mass per unit span	m	1.2942 kg/m
Young's modulus	E	70×10^9 Pa
Density	ρ_s	2700 kg/m^3
Air density	ρ_∞	1.224 kg/m^3
Store mass	M_s	1.578 kg
Store inertia	I_s	0.0185 kg·m^2

Table 4.3: Natural frequencies of the first three modes for different store locations

Location of Store (m)	First Bending [Hz]	Second Bending [Hz]	Torsional [Hz]
0.000	6.76	42.40	78.96
0.432	6.26	26.77	40.22
1.219	2.97	25.61	23.82

The results presented in Table 4.4 clearly demonstrate a significant influence of store placement on the flutter stability of the wing. The flutter speed initially increases as the external store moves outward from the root, reaching its maximum at the mid-span location (0.432, m). This optimal location enhances structural inertia sufficiently to stabilize flutter modes without excessively reducing structural stiffness. However, further spanwise movement towards the wing tip significantly decreases flutter stability, resulting in the lowest flutter speed at the tip location. This observed behavior arises from the complex interplay between inertia distribution, aerodynamic forces, and structural flexibility. At mid-span, inertia beneficially affects bending-torsion coupling, delaying flutter onset. Conversely, at the tip, reduced stiffness and unfa-

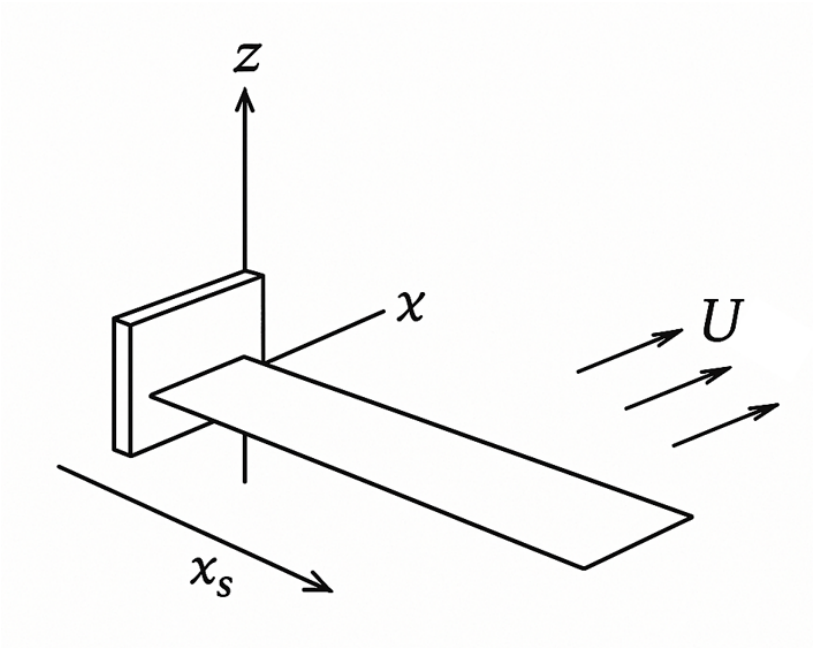

Figure 4.4: Plate geometry, boundary conditions, and store attachment locations X_s.

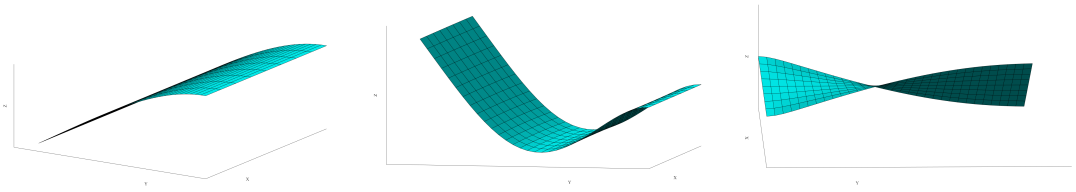

(a) First bending 6.76 Hz (b) Second bending 42.4 Hz (c) First torsion 78.96 Hz

Figure 4.5: Mode shapes for clean configuration

vorable aerodynamic interaction significantly lower flutter stability margins. Therefore, strategic store placement becomes an essential design consideration to optimize aeroelastic performance and ensure structural safety. These findings underline the necessity of incorporating detailed aeroelastic analyses during payload integration phases. Proper understanding and management of external payload effects can significantly enhance aircraft structural integrity, safety margins, and overall operational efficiency.

The analysis demonstrated that spanwise store placement Figure 4.5 exerts a significant influence on flutter stability of a clamped-wing configuration. When the store is mounted at the wing root, the flutter speed of 96.3,m/s reflects the baseline

Table 4.4: Predicted flutter speeds and frequencies for different store locations

Location of Store (m)	Flutter Speed (m/s)	Flutter Frequency (Hz)
0	96.3	24.6
0.432	116.4	28.2
1.219	90.8	24.4

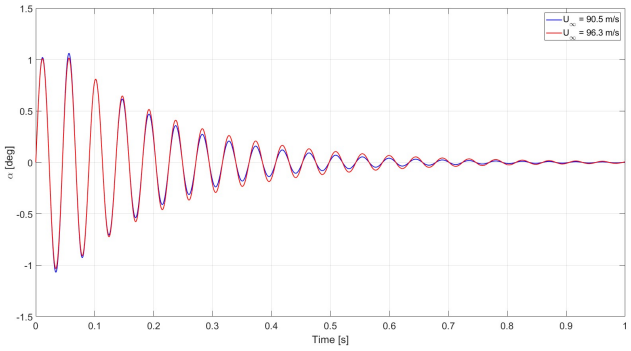

Figure 4.6: Time history of twist angle without extra mass

stiffness-dominated condition. Moving the store to a mid-span position increases the flutter speed to 113.5,m/s, indicating that the added inertia at this location optimally interacts with bending–torsion coupling to delay flutter onset. In contrast, placing the store at the wing tip reduces the flutter speed to 90.8,m/s, Figure 4.6, Figure 4.7 and Figure 4.8 as the local reduction in structural stiffness coupled with unfavorable aerodynamic loading lowers stability margins. Results emphasize the critical importance of strategic payload positioning: situating stores near mid-span maximizes flutter resistance, whereas tip attachments degrade aeroelastic performance unless compensated by additional structural reinforcement or active control measures. From a design standpoint, integrating aeroelastic assessments early in the payload configuration process enables identification of optimal store locations, quantification of associated flutter risks, and informed tailoring of structural or control interventions to mitigate instability. Future investigations may address the effects of varying store masses, simultaneous multi-store arrangements, and implementation of adaptive control strategies to further enhance flutter resilience and overall operational reliability.

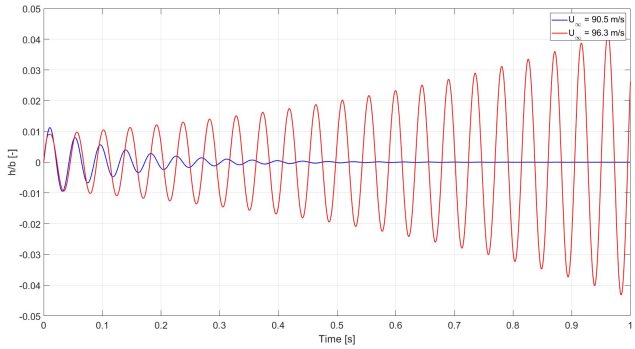

Figure 4.7: Time history of tip displacement without extra mass

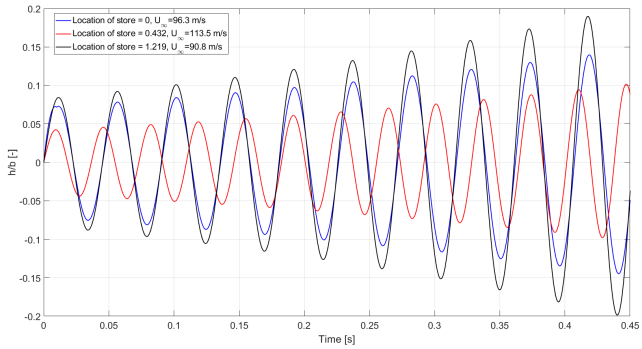

Figure 4.8: Time history of tip displacement with extra masses at different store locations

4.3 Chapter Summary and Concluding Remarks

In this chapter, the coupled UVLM–FEM solver has been applied to two essential aeroelastic scenarios: a clamped-wing flutter analysis and an external mass attachment study. The clamped-wing analysis—modeling a rectangular aluminum plate fixed at the root—yielded a critical flutter speed of 9.8 m/s and highlighted the dominant bending–torsion coupling mechanism. The external mass study then demonstrated how spanwise store placement can shift flutter margins by up to 17 m/s: mounting the store at mid-span (0.432 m) maximizes stability (113.5 m/s), whereas root (0 m, 96.3 m/s) and tip (1.219 m, 90.8 m/s) locations offer lower margins.These findings confirm the solver's ability to capture complex fluid–structure interactions and translate directly into design guidance. Strategic payload placement—favoring mid-span attachments—can substantially delay flutter onset, while tip-mounted stores

should be accompanied by structural reinforcement or active control to avoid early instability. By integrating such aeroelastic assessments early in the design and payload configuration processes, engineers can identify optimal store positions, quantify flutter risks, and implement targeted structural or control measures. Future work will extend this framework to address nonlinear boundary conditions, variable store masses, multi-store configurations, and adaptive flutter suppression strategies, further broadening the solver's applicability and reinforcing aircraft safety and performance.

CHAPTER 5

CONCLUSION AND FUTURE WORK

This thesis presents the development, validation, and application of an efficient, mid-fidelity computational aeroelastic solver, *AeroWing*, which couples an Unsteady Vortex Lattice Method (UVLM) aerodynamic code with a Finite Element Method (FEM) structural code. By retaining only the first three bending and torsion modes, the solver strikes a careful balance between computational speed and predictive accuracy. The key achievements of this work include:

- **Efficient Mid-Fidelity Framework:** Demonstrated that a reduced-order structural representation, when combined with UVLM-based aerodynamics, accurately captures flutter onset, limit cycle oscillations, and transient aeroelastic phenomena on standard desktop hardware within minutes.
- **Rigorous Validation:** Verified the solver against analytical solutions (e.g., Theodorsen's theory), independent FEM models, and wind-tunnel experiments, achieving flutter-speed predictions and mode-shape agreements within single-digit percentage deviations.
- **Parametric Sensitivity Studies:** Quantified the influence of plate thickness, spanwise store placement, and boundary conditions on aeroelastic stability. Results highlighted up to an order-of-magnitude change in critical flutter speeds and revealed mid-span payload attachment as the optimal configuration for maximizing flutter resistance.
- **Practical Design Guidance:** Translated solver outputs into actionable recommendations for preliminary aircraft design - enabling engineers to perform rapid *what-if* scenarios and early-stage aeroelastic assessments before resorting

to full-scale CFD/FEM or experimental campaigns.

The success of this mid-fidelity approach underscores its potential as a design-stage tool, closing the gap between quick analytical estimates and resource-intensive high-fidelity simulations.

5.1 Future Work Suggestions

Looking forward, the goal is to bring this capability into the third dimension. Real wings and blades are not flat plates: they twist, camber, and host intricate internal structures. To bridge that gap, a 3-D panel-based UVLM implementation can be used that can handle arbitrary planforms and enforce Kutta conditions along curved trailing edges. Paired with this aerodynamic upgrade, the structural solver will evolve to shell or solid elements, capturing out-of-plane bending, shear, and realistic wing-box cross sections. Moving to three dimensions will require a robust fluid–structure interaction loop: aerodynamic loads must update the structural state each time step, and deformations must feed back cleanly to the aerodynamic mesh. The numerical approach can be built on the existing predictor–corrector framework, adding under-relaxation or quasi-Newton accelerators as needed to maintain numerical stability. Validation against classic 3D benchmarks, such as the AGARD 445.6 and Goland Wings, will be central to the research efforts. By matching flutter speeds, mode shapes, and hysteresis patterns from wind-tunnel tests, a sensitivity analysis can be done to calibrate discretization choices and to build user trust. Beyond geometric fidelity, one aim to enrich the physics by including geometric nonlinearities and simple viscous corrections. Handling large deformations, variable damping rates, and low-Reynolds-number effects will open the door to applications in high-altitude UAVs, small-scale energy harvesters, and novel morphing surfaces. In short, the road map ahead will transform the solver from a fast 2D demonstrator into a comprehensive 3D aeroelastic analysis tool - one that sits between quick preliminary estimates and full-fledged CFD/FEM simulations, empowering engineers to innovate with confidence.

REFERENCES

[1] A. R. Collar, "The aeroelastic triangle," *Royal Aeronautical Society Journal*, vol. 50, pp. 9–14, 1946.

[2] J. Katz and A. Plotkin, *Low-Speed Aerodynamics: From Wing Theory to Panel Methods*. Cambridge, UK: Cambridge University Press, 2nd edition ed., 2001.

[3] J. R. Wright and J. E. Cooper, *Introduction to Aircraft Aeroelasticity and Loads*. John Wiley & Sons, 2nd edition ed., 2016.

[4] Z. Yuan and J. Dong, *Introduction to Aeroelasticity*. Berlin, Germany: Springer, 1st edition ed., 2013.

[5] E. Dowell and J. Thomas, "Efficient method for limit cycle flutter analysis based on nonlinear aerodynamic reduced-order models," *AIAA Journal*, vol. 50, no. 5, pp. 1019–1028, 2012.

[6] R. L. Bisplinghoff, H. Ashley, and R. L. Halfman, *Aeroelasticity*. Dover Publications, 1996.

[7] E. Dowell, *A Modern Course in Aeroelasticity*. Springer, 1975.

[8] D. H. Hodges and G. A. Pierce, *Introduction to Structural Dynamics and Aeroelasticity*. Cambridge University Press, 2003.

[9] E. H. Dowell, H. C. C. Jr., R. H. Scanlan, and F. Sisto, *A Modern Course in Aeroelasticity*. Alphen aan den Rijn, The Netherlands: Sijthoff & Noordhoff, 1978.

[10] F. Bramwell, "Flutter analysis in early aviation," *Royal Aeronautical Society Proceedings*, vol. 28, pp. 15–27, 1924.

[11] P. P. Friedmann and M. Torres, "Nonlinear aeroelasticity and limit cycle oscillations of high-aspect-ratio wings," *Progress in Aerospace Sciences*, vol. 107, pp. 1–37, 2019.

[12] G. Dimitriadis, “Flexible wing dynamics in unmanned aerial systems,” *Progress in Aerospace Sciences*, vol. 129, pp. 1–21, 2021.

[13] E. H. Dowell and J. P. Thomas, *Flutter and Other Aeroelastic Instabilities*. Springer, 2017.

[14] M. Krack and G. Dimitriadis, “Flutter analysis and limit cycle oscillations in nonlinear aeroelastic systems,” *Journal of Sound and Vibration*, vol. 490, p. 115684, 2021.

[15] Federal Aviation Administration, “Guidance on aeroelastic analysis for aircraft certification,” 2020. FAA Advisory Circular or Technical Standard Order on Aeroelasticity.

[16] European Union Aviation Safety Agency, “Certification specifications for large aeroplanes: Aeroelastic analysis requirements,” 2019. EASA Certification Specifications (CS-25), Section on Aeroelasticity.

[17] I. E. Garrick, “On some reciprocal relations in the theory of nonstationary flows,” *NACA Report*, vol. 629, pp. 1–24, 1945.

[18] S. Goldstein, *Modern Developments in Fluid Mechanics*. Clarendon Press, 1935.

[19] T. Theodorsen, *General Theory of Aerodynamic Instability and the Mechanism of Flutter*. NACA Report, 1935.

[20] P. P. Friedmann, “Transonic aeroelastic phenomena in turbomachines and wings,” *AIAA Journal*, vol. 52, pp. 893–931, 2014.

[21] H. J. Hassig, “An approximate true damping solution of the flutter equation by a method of successive determinants,” *Journal of Aircraft*, vol. 8, no. 11, pp. 885–889, 1971.

[22] O. O. Bendiksen, “A new approach to flutter analysis by a generalized method of characteristics,” *Journal of Aircraft*, vol. 22, no. 1, pp. 37–44, 1985.

[23] A. H. Nayfeh, “Nonlinear aeroelasticity and its applications,” *AIAA Journal*, vol. 17, no. 6, pp. 497–505, 1979.

[24] D. Tang and E. Dowell, "Limit cycle oscillations for high-aspect-ratio wings," *Journal of Fluids and Structures*, vol. 10, no. 8, pp. 873–896, 1996.

[25] B. H. K. Lee and S. J. Price, "Nonlinear aeroelastic analysis of limit cycle oscillations for aircraft with external stores," *Journal of Sound and Vibration*, vol. 222, no. 5, pp. 893–917, 1999.

[26] P. J. Richards and T. Walker, "Advances in fluid-structure interaction modelling," *International Journal of Aerodynamics*, vol. 6, pp. 75–104, 2017.

[27] S. L. Brunton and J. N. Kutz, *Dynamic Mode Decomposition: Data-Driven Modeling of Complex Systems*. SIAM, 2016.

[28] T. P. Sapsis, "Machine learning for stochastic and complex systems," *Nature Computational Science*, vol. 1, pp. 30–41, 2020.

[29] E. Albano and W. P. Rodden, "A doublet-lattice method for calculating lift distributions on oscillating surfaces in subsonic flows," *AIAA Journal*, vol. 7, pp. 279–285, 1969.

[30] W. P. Rodden and E. H. Johnson, "The unsteady aerodynamics of rotating and flexible aircraft," *AIAA Journal*, vol. 8, no. 10, pp. 1781–1786, 1970.

[31] G. Batchelor, *An Introduction to Fluid Dynamics*. Cambridge University Press, 1967.

[32] H. Ashley and R. Bisplinghoff, *Aeroelasticity*. New York, USA: Dover Publications, 1st edition ed., 1965.

[33] H. Lamb, *Hydrodynamics*. Cambridge University Press, 6th ed., 1932.

[34] C. Oseen, "Contributions to the theory of stationary and slow moving fluids," *Arkiv för Matematik, Astronomi och Fysik*, vol. 7, pp. 1–52, 1912.

[35] D. Burnham and P. Hallock, "Vortex model representations of free-vortex wakes," tech. rep., NASA Technical Paper 2107, 1982.

[36] G. Vatistas, T. Sankar, and C. Nguyen, "A simpler model for concentrated vortices," *Experiments in Fluids*, vol. 11, no. 1, pp. 73–76, 1991.

[37] Y. C. Fung, *An Introduction to the Theory of Aeroelasticity*. Dover Publications, 2002.

[38] E. H. Dowell, *A Modern Course in Aeroelasticity*. Springer, 5th edition ed., 2015.

[39] J. G. Leishman, *Principles of Helicopter Aerodynamics*. Cambridge University Press, 2nd edition ed., 2006.

[40] I. E. Garrick and W. H. Reid, "Historical development of aircraft flutter," *Journal of Aircraft*, vol. 20, no. 3, pp. 191–202, 1993.

[41] X. Amandolese, S. Michelin, and M. Choquel, "Low speed flutter and limit cycle oscillations of a two-degree-of-freedom flat plate in a wind tunnel," *Journal of Fluids and Structures*, vol. 35, pp. 105–119, 2012.

[42] S. A. Fazelzadeh, A. Mazidi, and H. Kalantari, "Bending-torsional flutter of wings with an attached mass subjected to a follower force," *Journal of Sound and Vibration*, vol. 323, no. 1-2, pp. 148–162, 2009.